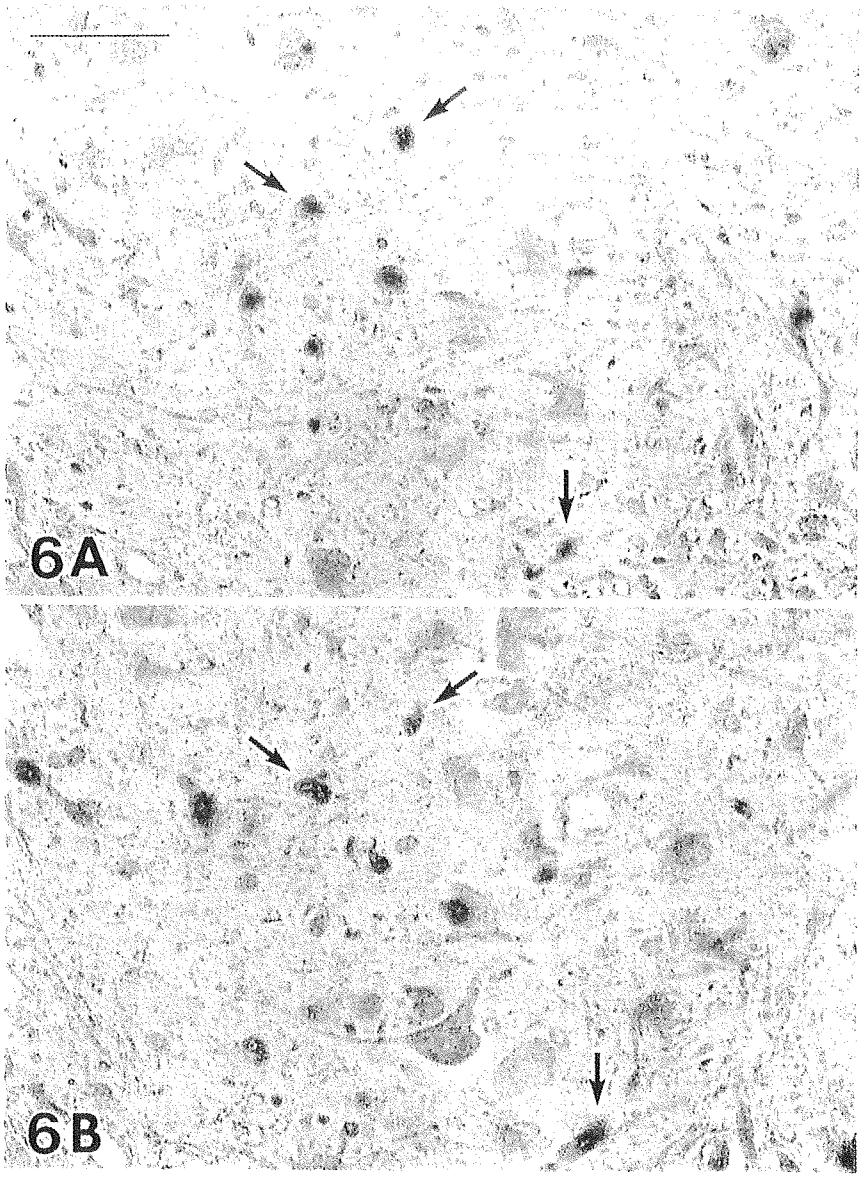

Fig. 6 Serial sections of the spinal anterior horn in a transgenic rat expressing human SOD1 with an H46R mutation immunostained with antibodies against SOD1 (**A**) and Prx2 (**B**). Round and sausage-like LBHIs in the neuropil are positive for both SOD1 and Prx2 (*arrows*) (*SOD1* superoxide dismutase1, *LBHI* Lewy body-like hyaline inclusion, *Prx2* peroxiredoxin2). *Bar* **A** (also for **B**) 50 μm

and GPx1 within the neuronal cytoplasm are extremely effective regulators of the redox system, our immunohistochemical finding that almost all of the normal spinal motor neurons co-expressed both Prx2 and GPx1 confirms that these motor neurons maintain themselves using the intracellular Prx2/GPx1 system, that is, the redox system.

As expected [12, 13, 16, 27, 30], SOD1 protein (probably the mutant form) was found to aggregate in the anterior horn cells as neuronal LBHIs in FALS patients with SOD1 gene mutations and transgenic rats expressing human SOD1 with H46R and G93A mutations. Intense co-expression of SOD1, Prx2, and GPx1 in neuronal LBHIs in both diseases was evident. To eliminate ROSs, SOD1-mutated motor neurons in mutant SOD1-linked FALS and transgenic rats (G46R and G93A) induce mutant/wild-type SOD1 as an antioxidant system and Prx2/GPx1 as a redox system. In this in vivo milieu where mutant SOD1 exists, Prx2 and GPx1 would aberrantly interact with the mutant SOD1, which is assumed to aggregate easily by itself [8]. Among the multiple theories of how mutant SOD1 contributes to motor neuron death in mutant SOD1-related FALS and transgenic animal models expressing human mutant SOD1, the aggregation of mutant SOD1 in neurons leads to part of the mutant SOD1-mediated toxicity through the formation of advanced glycation endproduct-modified SOD1 that is insoluble and cytotoxic [16]. Our recent study of FALS patients with a two-base pair deletion at codon 126 of the SOD1 gene (Oki family) and G85R transgenic mice has revealed that not only does mutant SOD1 provoke inclusion formation, but that normal SOD1 also co-aggregates in these inclusions [3]. Together with the facts that there are neuronal LBHIs positive for

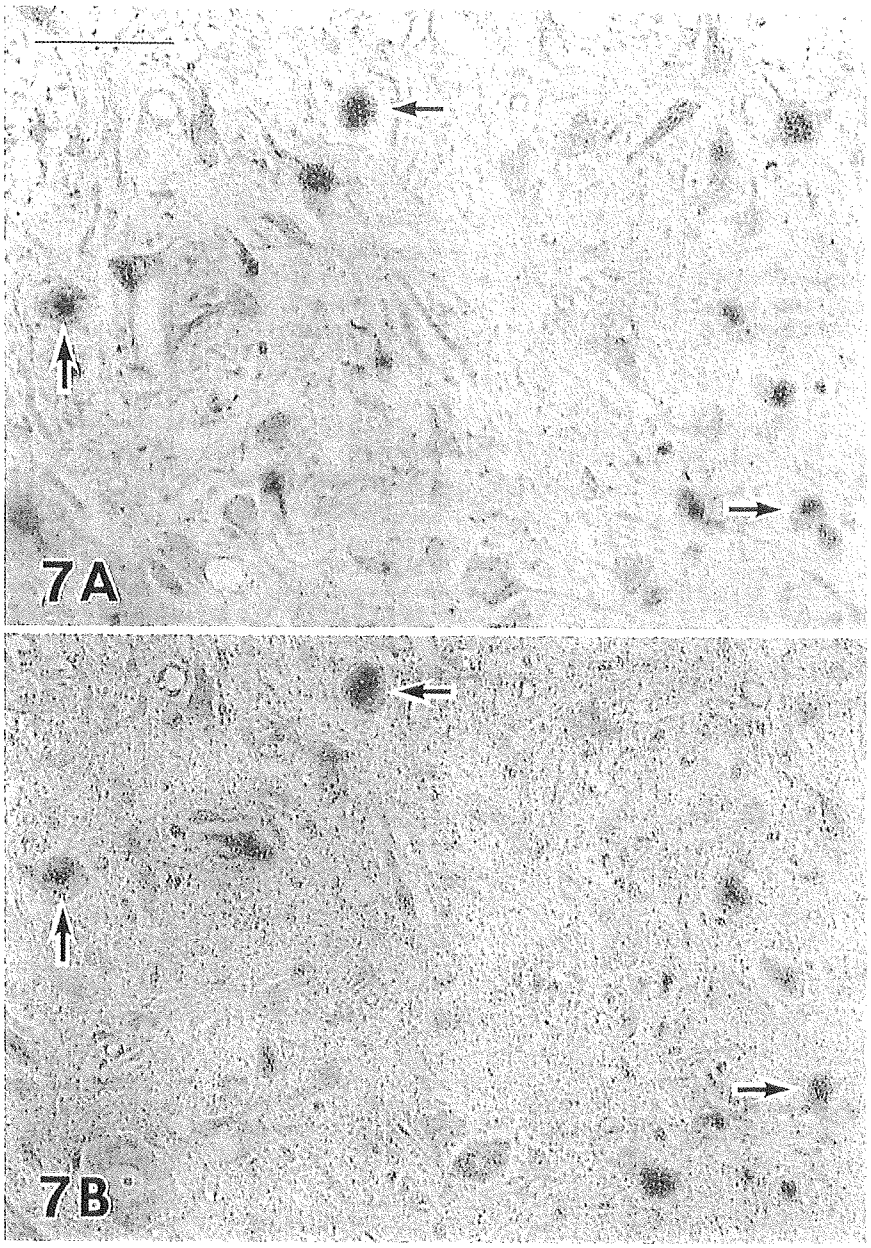

Fig. 7 Serial sections of the spinal anterior horn in a transgenic rat expressing human SOD1 with an H46R mutation immunostained with antibodies against SOD1 (**A**) and GPx1 (**B**). Round LBHIs in the neuropil are positive for both SOD1 and GPx1 (*arrows*) (*SOD1* superoxide dismutase1, *LBHI* Lewy body-like hyaline inclusion, *GPx1* glutathione peroxidase1). *Bar* **A** (also for **B**) 50 μm

SOD1, Prx2, and GPx1 in the milieu where mutant SOD1 exists but no LBHIs (no aggregations) exist under physiological conditions, our study demonstrates an aberrant interaction of Prx2/GPx1 with mutant SOD1, the aggregation of which results in neuronal LBHIs. In addition, intra-inclusional co-aggregation of Prx2/GPx1 with mutant SOD1 causes the intracytoplasmic reduction of Prx2/GPx1, thereby reducing the availability of the redox system. A similar aberrant interaction of the copper chaperone for SOD (CCS) and SOD1 (probably CCS-mutant SOD1) also occurs in the formation of the neuronal LBHIs in mutant SOD1-linked FALS [19] and the mutant SOD1 transgenic mouse model [32]. Such sequestration into LBHIs has also been observed for normal cytosolic constitutive proteins including tubulin and tau protein, as well as neuron-specific constitutive proteins containing phosphorylated neurofilament proteins (NFP), nonphosphorylated NFP, synaptophysin, and neuron-specific enolase [13, 17, 18]; this results in partial impairment of the maintenance of cell metabolism [13, 17, 18]. Although we cannot readily compare the sequestration of normal constitutive proteins with the aberrant interaction of cytotoxic mutant SOD1 with Prx2/GPx1 directly regulating a redox system, our finding leads us to speculate that not only co-aggregation of Prx2/GPx1 and SOD1 into LBHIs, but also intracytoplasmic reduction of Prx2/GPx1 in both diseases may partly contribute to the breakdown of the redox system itself in these SOD1-mutated neurons, and this may be one of the

endogenous mechanisms that accelerate neuronal death. This hypothesis would appear to be compatible with the aggregation toxicity theory. It remains to be determined whether this aberrant interaction of Prx2/GPx1 with mutant SOD1 is a direct or an indirect effect based on the pathogenesis of SOD1-mutated FALS disease itself or whether Prx2 and GPx1 play a primary or a secondary role to mutant SOD1. Consequently, we would like to emphasize that the aberrant interaction and co-aggregation of Prx2/GPx1 and SOD1 (probably Prx2/GPx1 and mutant SOD1) in FALS patients with SOD1 gene mutations and transgenic rats expressing human SOD1 mutations may amplify a more marked mutant SOD1-mediated toxicity.

Acknowledgements This study was supported in part by a Grant-in-Aid for Scientific Research (c) (2) from the Ministry of Education, Culture, Sports, Science and Technology of Japan (S.K.: 13680821) and by a Grant from the Ministry of Health, Labour and Welfare of Japan (S.K. and Y.I.).

References

1. Asayama K, Burr IM (1984) Joint purification of mangano and cuprozinc superoxide dismutases from a single source: a simplified method. Anal Biochem 136:336–339
2. Asayama K, Yokota S, Dobashi K, Hayashibe H, Kawaoi A, Nakazawa S (1994) Purification and immunoelectron microscopic localization of cellular glutathion peroxidase in rat hepatocytes: quantitative analysis by postembedding method. Histochemistry 102:213–219
3. Bruijn LI, Houseweart MK, Kato S, Anderson KL, Anderson SD, Ohama E, Reaume AG, Scott RW, Cleveland DW (1998) Aggregation and motor neuron toxicity of an ALS-linked SOD1 mutant independent from wild-type SOD1. Science 281: 1851–1854
4. Chae HZ, Kim IH, Kim K, Rhee SG (1993) Cloning, sequencing, and mutation of thiol-specific antioxidant gene of *Saccharomyces cerevisiae*. J Biol Chem 268:16815–16821
5. Chae HZ, Chung SJ, Rhee SG (1994) Thioredoxin-dependent peroxide reductase from yeast. J Biol Chem 269:27670–27678
6. Chae HZ, Robison K, Poole LB, Church G, Storz G, Rhee SG (1994) Cloning and sequencing of thiol-specific antioxidant from mammalian brain: alkyl hydroperoxide reductase and thiol-specific antioxidant define a large family of antioxidant enzymes. Proc Natl Acad Sci USA 91:7017–7021
7. De Haan JB, Bladier C, Griffiths P, Kelner M, O'Shea RD, Cheung NS, Bronson RT, Silvestro MJ, Wild S, Zheng SS, Beart PM, Hertzog PJ, Kola I (1998) Mice with a homozygous null mutation for the most abundant glutathione peroxidase, Gpx1, show increased susceptibility to the oxidative stress-inducing agents paraquat and hydrogen peroxide. J Biol Chem 273:22528–22536
8. Durham HD, Roy J, Dong L, Figlewicz DA (1997) Aggregation of mutant Cu/Zn superoxide dismutase proteins in a culture model of ALS. J Neuropathol Exp Neurol 56:523–530
9. Fridovich I (1986) Superoxide dismutases. Adv Enzymol Relat Area Mol Biol 58:61–97
10. Jin D-Y, Chae HZ, Rhee SG, Jeang K-T (1997) Regulatory role for a novel human thioredoxin peroxidase in NF-kappaB activation. J Biol Chem 272:30952–30961
11. Kato S, Shimoda M, Morita T, Watanabe Y, Nakashima K, Takahashi K, Ohama E (1996) Neuropathology of familial ALS with a mutation of the superoxide dismutase 1 gene. In: Nakano I, Hirano A (eds) Amyotrophic lateral sclerosis: progress and perspectives in basic research and clinical application. Elsevier Science, Amsterdam, pp 117–122
12. Kato S, Shimoda M, Watanabe Y, Nakashima K, Takahashi K, Ohama E (1996) Familial amyotrophic lateral sclerosis with a two base pair deletion in superoxide dismutase 1 gene: multisystem degeneration with intracytoplasmic hyaline inclusions in astrocytes. J Neuropathol Exp Neurol 55:1089–1101
13. Kato S, Hayashi H, Nakashima K, Nanba E, Kato M, Hirano A, Nakano I, Asayama K, Ohama E (1997) Pathological characterization of astrocytic hyaline inclusions in familial amyotrophic lateral sclerosis. Am J Pathol 151:611–620
14. Kato S, Horiuchi S, Nakashima K, Hirano A, Shibata N, Nakano I, Saito M, Kato M, Asayama K, Ohama E (1999) Astrocytic hyaline inclusions contain advanced glycation endproducts in familial amyotrophic lateral sclerosis with superoxide dismutase 1 gene mutation: immunohistochemical and immunoelectron microscopical analyses. Acta Neuropathol 97: 260–266
15. Kato S, Saito M, Hirano A, Ohama E (1999) Recent advances in research on neuropathological aspects of familial amyotrophic lateral sclerosis with superoxide dismutase 1 gene mutations: neuronal Lewy body-like hyaline inclusions and astrocytic hyaline inclusions. Histol Histopathol 14:973–989
16. Kato S, Horiuchi S, Liu J, Cleveland DW, Shibata N, Nakashima K, Nagai R, Hirano A, Takikawa M, Kato M, Nakano I, Ohama E (2000) Advanced glycation endproduct-modified superoxide dismutase-1 (SOD1)-positive inclusions are common to familial amyotrophic lateral sclerosis patients with SOD1 gene mutations and transgenic mice expressing human SOD1 with G85R mutation. Acta Neuropathol 100:490–505
17. Kato S, Takikawa M, Nakashima K, Hirano A, Cleveland DW, Kusaka H, Shibata N, Kato M, Nakano I, Ohama E (2000) New consensus research on neuropathological aspects of familial amyotrophic lateral sclerosis with superoxide dismutase 1 (SOD1) gene mutations: inclusions containing SOD1 in neurons and astrocytes. Amyotroph Lateral Scler Other Motor Neuron Disord 1:163–184
18. Kato S, Nakashima K, Horiuchi S, Nagai R, Cleveland DW, Liu J, Hirano A, Takikawa M, Kato M, Nakano I, Sakoda S, Asayama K, Ohama E (2001) Formation of advanced glycation end-product-modified superoxide dismutase-1 (SOD1) is one of the mechanisms responsible for inclusions common to familial amyotrophic lateral sclerosis patients with SOD1 gene mutation, and transgenic mice expressing human SOD1 gene mutation. Neuropathology 21:67–81
19. Kato S, Sumi-Akamaru H, Fujimura H, Sakoda S, Kato M, Hirano A, Takikawa M, Ohama E (2001) Copper chaperone for superoxide dismutase co-aggregates with superoxide dismutase 1 (SOD1) in neuronal Lewy body-like hyaline inclusions: an immunohistochemical study on familial amyotrophic lateral sclerosis with SOD1 gene mutation. Acta Neuropathol 102:233–238
20. Kato T, Hirano A, Kurland LT (1987) Asymmetric involvement of the spinal cord involving both large and small anterior horn cells in a case of familial amyotrophic lateral sclerosis. Clin Neuropathol 6:67–70
21. Kosower NS, Kosower EM (1978) The glutathione status of cells. Int Rev Cytol 54:109–160
22. Kurland LT, Mulder DW (1955) Epidemiologic investigations of amyotrophic lateral sclerosis. II. Familial aggregations indicative of dominant inheritance. Neurology 5:249–268
23. Matsumoto A, Okado A, Fujii T, Fujii J, Egashira M, Niikawa N, Taniguchi N (1999) Cloning of the peroxiredoxin gene family in rats and characterization of the fourth member. FEBS Lett 443:246–250
24. Meister A, Anderson ME (1983) Glutathione. Annu Rev Biochem 52:711–760
25. Mills GC (1957) Hemoglobin catabolism. 1. Glutathione peroxidase, an erythrocyte enzyme which protects hemoglobin from oxidative breakdown. J Biol Chem 229:189–197
26. Mu ZM, Yin XY, Prochownik EV (2002) Pag, a putative tumor suppressor, interacts with the Myc Box II domain of c-Myc and selectively alters its biological function and target gene expression. J Biol Chem 277:43175–43184

27. Nagai M, Aoki M, Miyoshi I, Kato M, Pasinelli P, Kasai N, Brown RH Jr, Itoyama Y (2001) Rats expressing human cytosolic copper-zinc superoxide dismutase transgenes with amyotrophic lateral sclerosis: associated mutations develop motor neuron disease. J Neurosci 21:9246–9254
28. Nakano I, Hirano A, Kurland LT, Mulder DW, Holley PW, Saccomanno G (1984) Familial amyotrophic lateral sclerosis. Neuropathology of two brothers in American "C" family. Neurol Med (Tokyo) 20:458–471
29. Sen CK, Packer L (1996) Antioxidant and redox regulation of gene transcription. FASEB J 10:709–720
30. Shibata N, Hirano A, Kobayashi M, Siddique T, Deng HX, Hung WY, Kato T, Asayama K (1996) Intense superoxide dismutase-1 immunoreactivity in intracytoplasmic hyaline inclusions of familial amyotrophic lateral sclerosis with posterior column involvement. J Neuropathol Exp Neurol 55:481–490
31. Takahashi K, Nakamura H, Okada E (1972) Hereditary amyotrophic lateral sclerosis. Histochemical and electron microscopic study of hyaline inclusions in motor neurons. Arch Neurol 27:292–299
32. Watanabe M, Dykes-Hoberg M, Culotta VC, Price DL, Wong PC, Rothstein JD (2001) Histological evidence of protein aggregation in mutant SOD1 transgenic mice and in amyotrophic lateral sclerosis neural tissues. Neurobiol Dis 8:933–941
33. Wen ST, Van Etten RA (1997) The PAG gene product, a stress-induced protein with antioxidant properties, is an Abl SH3-binding protein and a physiological inhibitor of c-Abl tyrosine kinase activity. Genes Dev 11:2456–2467

THE JOURNAL OF BIOLOGICAL CHEMISTRY

Vol. 280, No. 6, Issue of February 11, pp. 5061–5070, 2005
Printed in U.S.A.

Different Immunoreactivity against Monoclonal Antibodies between Wild-type and Mutant Copper/Zinc Superoxide Dismutase Linked to Amyotrophic Lateral Sclerosis*

Received for publication, June 2, 2004, and in revised form, October 29, 2004
Published, JBC Papers in Press, November 2, 2004, DOI 10.1074/jbc.M406106200

Noriko Fujiwara‡, Yasuhide Miyamoto§, Kyoko Ogasahara¶, Motoko Takahashi§, Takahisa Ikegami¶, Rina Takamiya§, Keiichiro Suzuki‡, and Naoyuki Taniguchi§‖

From the ‡Department of Biochemistry, Hyogo College of Medicine, 1-1 Mukogawa-cho, Nishinomiya, Hyogo 663-8501, the §Department of Biochemistry, Osaka University Medical School & Graduate School of Medicine, 2-2 Yamadaoka, Suita, Osaka 565-0871, and ¶Institute of Protein Research, Osaka University, 3-2 Yamadaoka, Suita, Osaka 565-0871, Japan

Although more than 100 mutations have been identified in the copper/zinc superoxide dismutase (Cu/Zn-SOD) in familial amyotrophic lateral sclerosis (FALS), the mechanism responsible for FALS remains unclear. The finding of the present study shows that FALS-causing mutant Cu/Zn-SOD proteins (FALS mutant SODs), but not wild-type SOD, are barely detected by three monoclonal antibodies (mAbs) in Western blot analyses. The enzyme-linked immunosorbent assay for denatured FALS mutant SODs by dithiothreitol, SDS, or heat treatment also showed a lowered immunoreactivity against the mAbs compared with wild-type SOD. Because all the epitopes of these mAbs are mapped within the Greek key loop (residues 102–115 in human Cu/Zn-SOD), these data suggest that different conformational changes occur in the loop between wild-type and FALS mutant SODs during the unfolding process. Circular dichroism measurements revealed that the FALS mutant SODs are sensitive to denaturation by dithiothreitol, SDS, or heat treatment, but these results do not completely explain the different recognition by the mAbs between wild-type and FALS mutant SODs under the denatured conditions. The study on the conformational changes in local areas monitoring with mAbs may provide a new insight into the etiology of FALS.

Amyotrophic lateral sclerosis (ALS)[1] is a neurological disease characterized by selective motor neurons in the brain and spinal cord. Although most reported cases are sporadic ALS, 5–10% are familial ALS (FALS). About 20–25% of FALS cases have been shown to be associated with mutations in the copper/zinc superoxide dismutase (Cu/Zn-SOD) gene, *SOD1* on chromosome 21q22.1 (1, 2). Cu/Zn-SOD is a homodimer containing one copper ion and one zinc ion in each 16-kDa subunit. Cu/Zn-SOD catalyzes the disproportionation of superoxide anion (O_2^-) into O_2 and H_2O_2 and has been shown to play a protective role in cells against oxidative stress. To date, more than 100 FALS-causing mutations in the Cu/Zn-SOD, which consists of 153 amino acids, have been identified (3). Although some FALS causing-mutant Cu/Zn-SOD proteins (FALS mutant SODs) show less enzymatic activities, many retain full activity (4). Several lines of transgenic mice that express mutant human *SOD1* linked with FALS developed progressive neurodegeneration and a phenotype that clearly resembles human FALS (5, 6) despite having higher SOD activity. In contrast, *SOD1*-knock out mice do not exhibit motor neuron dysfunction (7). These findings suggest that this disease is the result of a toxic gain of function but not a loss in SOD activity. Several different hypotheses have been proposed to explain the toxic gain of function, including the production of ROS, mitochondrial defects, glutamate-induced excitotoxicity, neurofilament inclusions, and the formation of intracellular toxic protein aggregates (reviewed in Ref. 8). However, the mechanism by which FALS mutant SODs causes motor neuron degeneration is not completely understood.

The tertiary structure of Cu/Zn-SOD is characterized by the presence of a Greek key β-barrel containing an internal disulfide bond between Cys-57 and Cys-146 (9, 10), both of which contribute to its high stability. On the other hand, various FALS mutant SODs show a decreased stability and a lower level of metallation (4, 11, 12). Several reports, including ours (Fig. 1),[2] reported that FALS mutant SODs exhibit an accelerated turnover or an increased susceptibility to degradation in proteasome (13, 14) and suggest that unfolding or conformational perturbations of mutant SOD proteins occur *in vivo*. Niwa *et al.* (15) reported that Dorfin, a RING finger-type ubiquitin-protein isopeptide ligase (E3) ubiquitinates the FALS mutant SODs but not wild-type Cu/Zn-SOD, suggesting that FALS mutant SODs have a unique structure that can be recognized by Dorfin. We reported previously that FALS mutant SODs are more susceptible to glycation or fructation (16) and that they form aggregates at a higher rate than the wild-type SOD, when incubated in the presence of copper ions (4). These data also

* This work was supported by a grant from The Amyotrophic Lateral Sclerosis Association (United States), "Health and Labour Sciences Research Grants and Research on Measures for Intractable Diseases" from the Ministry of Health and Welfare Japan, by The Japan Foundation for Aging and Health, by the 21st Century Center of Excellence program from the Ministry of Education, Culture, Sports, Science, and Technology of Japan, and in part by a Hitech Research Center grant from the Ministry of Education, Science, and Culture of Japan, and the Japan Foundation for Applied Enzymology. The costs of publication of this article were defrayed in part by the payment of page charges. This article must therefore be hereby marked "*advertisement*" in accordance with 18 U.S.C. Section 1734 solely to indicate this fact.

‖ To whom all correspondence should be addressed: Dept. of Biochemistry, Osaka University Medical School & Graduate School of Medicine, 2-2 Yamadaoka, Suita, Osaka 565-0871, Japan. Tel.: 81-6-6879-3420; Fax: 81-6-6879-3429; E-mail: proftani@biochem.med.osaka-u.ac.jp.

[1] The abbreviations used are: ALS, amyotrophic lateral sclerosis; PBS, phosphate-buffered saline; DTT, dithiothreitol; 2-ME, 2-mercaptoethanol; ELISA, enzyme-linked immunosorbent assay; DNP, dinitrophenyl; SOD, superoxide dismutase; HPLC, high pressure liquid chromatography; FALS, familial amyotrophic lateral sclerosis; mAbs, monoclonal antibodies; WT, wild type; DNBS, 2,4-dinitrobenzenesulfonyl chloride; E3, ubiquitin-protein isopeptide ligase.

[2] N. Fujiwara, Y. Miyamoto, M. Takahashi, K. Suzuki, and N. Taniguchi, unpublished data.

indicate that FALS mutant SODs are susceptible to conformational changes. Inclusion bodies or aggregates that are immunoreactive to Cu/Zn-SOD were also observed in motor neurons and astrocytes of mice expressing mutant *SOD1*, as well as in human ALS cases linked to *SOD1* (17, 18). It has been reported recently that purified FALS mutant SODs also have a propensity to aggregate or to form amyloid-like fibrils (19–22). Therefore, it is possible that the pathology of FALS associated with mutant SODs may also involve aggregate formation and the degeneration of neuronal cells analogous to other neurodegenerative disorders such as Alzheimer's, Parkinson's, and Huntington's diseases, prion encephalopathies, and cystic fibrosis. Although it is generally thought that aggregation and amyloid formation require a conformational transition in a polypeptide chain from a native form to an improperly folded or mis-folded conformation in these diseases, the molecular basis of this remains unclear (23).

A monoclonal antibody (mAb) is a good tool for detecting structural differences and conformational changes in local areas within a protein molecule. A conformational transition of the prion protein has been detected by various mAbs (24–26). The pH-dependent conformational transition of the Alzheimer β-amyloid peptide was monitored by their mAbs (27). Inhibition of the fibrillar aggregation of the Alzheimer β-amyloid peptide (28) and inhibition of prion transmission (29) have also been reported, based on the use of mAbs.

The findings in the present study show that unfolded FALS mutant SODs show a lower immunoreactivity against three mAbs, compared with unfolded wild-type Cu/Zn-SOD in Western blots and ELISA. The epitope for all the mAbs was determined to be located in the Greek key loop VI. These data suggest that the denatured forms in this local area might well be different between wild-type and FALS mutant SODs because variations in recognition by the mAbs may indicate structural differences at this loop. This is the first demonstration of different recognition by mAbs between wild-type and FALS mutant SODs. The use of mAbs as a microprobe promises to contribute to the clarification of the structural mechanism by which FALS mutant SODs cause ALS.

EXPERIMENTAL PROCEDURES

Antibodies—Monoclonal antibodies against human Cu/Zn-SOD, N6, and SD-G6 were purchased from Panafarm (Kumamoto, Japan) and Sigma, respectively. 5c-10 was kindly provided by Dr. Uda (Hiroshima Prefecture University). Horseradish peroxidase-conjugated rabbit anti-goat IgG and goat anti-rabbit IgG were purchased from Dako (Denmark). Horseradish peroxidase-conjugated rabbit anti-mouse IgG was obtained from Promega. Picotan/picotein rabbit anti-DNP (IgG) was purchased from Cosmobio (Japan).

Cell Culture and Expression of Wild-type and Mutated Cu/Zn-SOD in Mammalian Cells—Neuro2a, a murine neuroblastoma cell line, was maintained in Dulbecco's modified Eagle's medium containing 100 units/ml penicillin and 100 μg/ml streptomycin supplemented with 10% heat-inactivated fetal bovine serum (Invitrogen) at 37 °C under an atmosphere of 95% air and 5% CO_2. Cells were transfected with the following wild-type and mutated SOD1 cDNAs transiently by Lipofectamine 2000, according to the manufacturer's instructions. The culturing of *Spodoptera frugiperda* (Sf21) cells and manipulations of the baculovirus were performed according to the procedures described by Piwnica-Worms (30). Sf21 cells were maintained in Grace's medium containing 3.3 mg/ml yeastolate, 3.3 mg/ml lactalbumin hydrolysate, and 50 μg/ml gentamycin supplemented with 10% heat-inactivated fetal bovine serum at 27 °C.

Mutagenesis and Construction of Plasmids—Point mutations were introduced into the human *SOD1* cDNA in Bluescript SK(+) using the overlap extension PCR mutagenesis procedure (31). The wild-type and mutant cDNAs were transferred into the *pcDNA3.1* mammalian expression vector and pVL1393 baculovirus expression vector between the BamHI and NotI sites. These constructs were confirmed by an automated DNA sequencing (Applied Biosystems model 310).

Western Blot Analysis—Proteins were subjected to SDS-PAGE and then transferred to a nitrocellulose membrane under semi-dry conditions by means of a Trans-blot (Bio-Rad). After blocking by incubation with 4% skim milk in Tris-buffered saline (20 mM Tris-HCl, pH 8.0, 0.15 M NaCl (TBS)) for 12 h at 4 °C, the membrane was incubated with a goat polyclonal antibody or monoclonal antibodies against human Cu/Zn-SOD (1000 ng/ml) in Tris-buffered saline containing 0.05% Tween 20 (TBS-T) and containing 1% skim milk for 2 h at room temperature. After washing with TBS-T, the membrane was incubated with peroxidase-conjugated rabbit anti-goat IgG (diluted 1:5000 in TBS-T containing 1% skim milk) or rabbit anti-mouse IgG (diluted 1:5000 in TBS-T containing 1% skim milk) for 2 h. After washing, the chemiluminescence method using an ECL kit (Amersham Biosciences) was employed to detect the peroxidase activity.

Overproduction and Purification of Wild-type and Mutant Cu/Zn-SOD Proteins—For the overproduction of Cu/Zn-SODs by the baculovirus/insect cells system, the wild-type cDNA and mutant cDNAs were ligated into the baculovirus transfer vector pVL1393 (Invitrogen) and cotransfected with BaculoGold (Pharmingen) into Sf21 cells using Lipofectin (Invitrogen). 0.5 mM $CuCl_2$ and 0.5 mM $ZnCl_2$ were added directly to the medium after viral infection. Purification of SOD proteins that were overproduced in Sf21 cells was carried out essentially as described previously (16) with minor modifications. $1–4 \times 10^8$ infected Sf21 cells were harvested and washed with PBS(−) and stored at −20 °C until used. The cells were homogenized in buffer A (2.5 mM potassium phosphate, pH 7.4) containing protein inhibitor mixture without EDTA (Roche Applied Science) and centrifuged at 100,000 × *g* for 30 min. The supernatant was applied to a DE52 cellulose column. After washing with buffer A, the bound proteins were eluted with a linear gradient of potassium phosphate from 2.5 to 200 mM. Fractions containing SOD protein were dialyzed on a PD10 column with buffer B (10 mM potassium phosphate, pH 7.4). The fractions were applied to a MonoQ-Sepharose column (Amersham Biosciences). After washing with buffer B, the bound proteins were eluted with a linear gradient of KCl (0–100 mM) in buffer B. Fractions containing SOD protein were dialyzed on a PD10 column with buffer C (10 mM potassium phosphate, pH 6.8) and applied to a hydroxyapatite type I column (Bio-Rad) to eliminate the minor contaminated proteins. After washing with buffer C, the bound proteins were eluted with a linear gradient of potassium phosphate from 10 to 300 mM. Fractions containing SOD protein were dialyzed on a PD10 column with 50 mM sodium bicarbonate, pH 9.6, and concentrated by Microcon YM-10 (Millipore). The MonoQ-Sepharose column and the hydroxyapatite column chromatography works were performed using AKTA Explorer 10S (Amersham Biosciences). The purity of SOD proteins was more than 99%, as judged by SDS-PAGE.

ELISA—Purified Cu/Zn-SOD proteins (0.25 mg/ml), with and without denaturing treatments in coating buffer (50 mM sodium bicarbonate, pH 9.6), were diluted to 1 μg/ml with coating buffer. 100 μl of the samples were added to each well of 96-well microplates (Maxisorp, Nunc), incubated overnight at 4 °C, washed three times with PBS containing 0.01% Tween 20 (PBS-T), and then blocked for 2 h at room temperature with 1% BSA in PBS. The plates were then washed three times with PBS-T, and 100 μl of monoclonal and goat polyclonal anti-human Cu/Zn-SOD antibodies (desired dilution in PBS-T) was added, followed by incubation for 1 h at room temperature. The plates were washed three times with PBS-T, and 100 μl of horseradish peroxidase-conjugated anti-mouse IgG (diluted 1:5000 in PBS-T) for monoclonal antibodies, anti-goat IgG (diluted 1:5000 in PBS-T) for a goat polyclonal antibody, or anti-rabbit IgG (diluted 1:5000 in PBS-T) for a rabbit polyclonal antibody was added and incubated for 1 h at room temperature. After washing five times with PBS-T, the plates were developed using 100 μl of *o*-phenylenediamine dihydrochloride solution, and the reaction was stopped with 25 μl of 2 M HCl. The absorbance of each well was determined at 490 nm with an Immunoreader NJ 200 (Intermed).

Preparation of DNP-SODs and Its ELISA—Preparation of DNP-SODs was performed according to a previous report by Little and Eisen (32) and the manufacturer's protocol of Picotan/picotein rabbit anti-DNP with minor modifications. Briefly, purified Cu/Zn-SOD proteins (0.25 mg/ml) were mixed with an equal volume of 2,4-dinitrobenzenesulfonyl chloride (DNBS) (1 mg/ml) in 0.5 M Na_2CO_3, pH 11.5, which had been incubated for 2 h at 37 °C, and diluted to various concentrations (0.05–1 μg/ml) in coating buffer. 100 μl of the samples were added to each well of 96-well microplates and incubated overnight at 4 °C. After washing, Picotan/picotein rabbit anti-DNP in PBS-T was directly added to the wells without a blocking step. The other steps were performed according to the method described above.

CD Analyses—Purified Cu/Zn-SOD proteins with and without denaturing treatments in coating buffer were subjected to CD spectral measurement using a Jasco J-720 spectropolarimeter (Jasco, Japan).

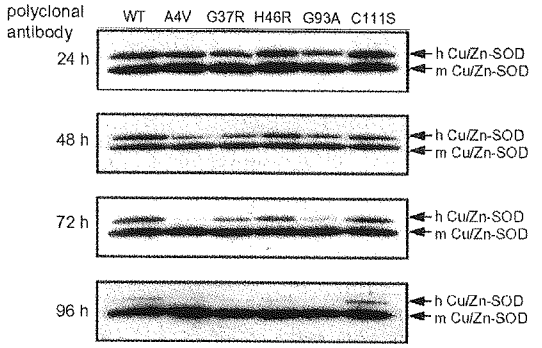

FIG. 1. **Estimation of wild-type and mutant Cu/Zn-SODs expressed in Neuro2a cells by Western blot analyses.** Two μg of mutant *SOD1* cDNAs as well as the wild-type *SOD1* cDNA were transiently transfected into Neuro2a cells by Lipofectamine. The cells were collected 24, 48, 72, and 96 h after transfection and dissolved in TNE buffer (50 mM Tris-HCl containing 1% Nonidet P-40 and 0.1 mM EDTA and protease inhibitor mixture (Roche Applied Science), pH 7.4) for 30 min on ice. After centrifugation (15,000 rpm) for 30 min, the proteins in the supernatant (20 μg) were subjected to SDS-PAGE. Human (*h*) and mouse (*m*) Cu/Zn-SODs in Neuro2a cells were detected by Western blot analyses using a polyclonal antibody.

The secondary structure was monitored over the wavelength range of 200–250 nm using a 0.1-cm path length cuvette at 25 °C. Eight scans were averaged for each sample; the averaged blank spectra of detergents dissolved into the same buffer solutions were subtracted. The CD data were expressed as mean residue ellipticity [θ] (degree cm^2/dmol). The protein concentrations under the CD measurements were 15 μM.

Epitope Mapping—0.5 mg of WT and A4V proteins were incubated at 0.25 mg/ml in 50 mM Tris-HCl, pH 8.6, containing 5 mM DTT, 7 M guanidine HCl, and 10 mM EDTA at 37 °C for 2 h. The free sulfhydryls were carboxymethylated by adding iodoacetic acid in the dark at room temperature for 30 min. After dialysis on a PD10 column with 50 mM Tris-HCl, pH 9.0, the proteins were digested with 0.25% (w/w) lysyl endopeptidase (Wako Pure Chemicals) at 37 °C for 16 h. The resulting peptides were applied to a reverse phase HPLC (AKTA Explorer 10S) at a flow rate of 1 ml/min on a Sephacryl peptide C18 column (4.6 × 250 mm, Amersham Biosciences). The peptides were separated by a linear gradient of 2–50% acetonitrile containing 0.05% trifluoroacetic acid. Peptides were detected by their absorbance at 215 nm. The peaks were subjected to mass spectrometry, amino acid sequencing, and ELISA. For the ELISA, the separated peptides or synthesized peptides were diluted with PBS(−), added to 96-well plates, and incubated for 2 h at room temperature. After washing, the first antibodies (mAbs) in PBS-T were directly added to the wells without a blocking step. The other steps were performed according to the method described above. Synthesized peptides were purchased from Sigma Genosys.

Protein Assay—Protein concentrations of crude samples were determined by using a protein assay kit (Bio-Rad) with bovine serum albumin as a standard. Purified Cu/Zn-SOD protein concentrations were estimated using a dimeric molar extinction at 280 nm of 10,800 M^{-1} cm^{-1} (33).

RESULTS

Typical FALS Mutant SODs Are Susceptible to Degradation in Neuro2a Cells—Mutant SOD1 cDNAs, A4V, G37R, H46R, G93A, and C111S were obtained using wild-type (WT) human SOD1 cDNA. The mutant C111S is not found in FALS, and Ser-111 is conserved in Cu/Zn-SOD in other mammalian species except for humans. It has also been reported that C111S is more thermally stable than the wild type (34, 35). Therefore, it would be expected that C111S does not cause ALS and can be used as a second control (wild type).

These mutant cDNAs, as well as the wild-type cDNA, were transiently transfected into Neuro2a cells. As shown in Fig. 1, although all human Cu/Zn-SOD proteins expressed the similar levels 24 h after transfection, A4V, G37R, and G93A were degraded more rapidly than H46R 48 h after transfection. The stability of the C111S protein was comparable with the wild type (WT), and both were more stable than the H46R protein.

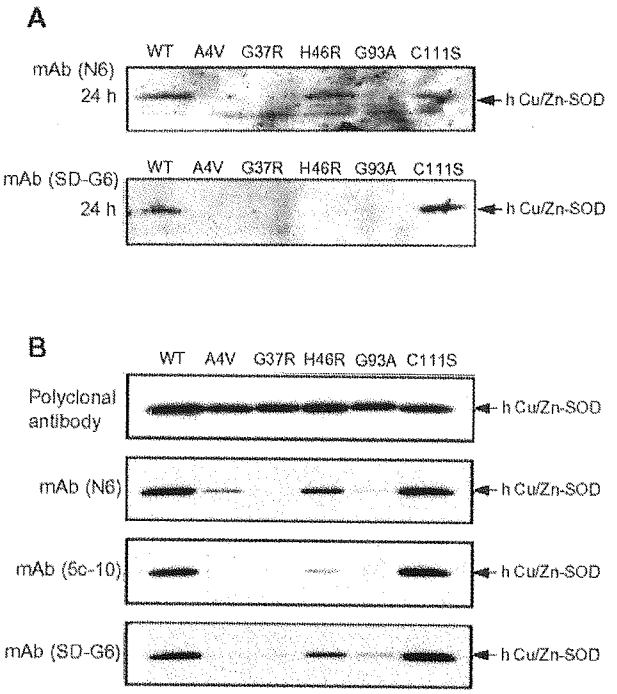

FIG. 2. **Western blot analyses of wild-type and mutant SODs detected by monoclonal antibodies.** *A*, human (*h*) Cu/Zn-SOD expressed in Neuro2a cells at 24 h after the transfection was detected by Western blot analyses using monoclonal antibodies. *B*, 30 ng of purified wild-type and mutant SODs were subjected to SDS-PAGE and were detected by Western blotting using monoclonal antibodies. Each nitrocellulose membrane, after reacting with the monoclonal antibodies, was de-probed by treatment with stripping buffer and re-incubated with a polyclonal antibody, and representative data are shown.

Endogenous mouse Cu/Zn-SOD was unchanged through the period of this observation. The addition of MG132, proteasome inhibitor, 24 h after transfection restored the protein levels of A4V, G37R, and G93A in a concentration-dependent manner (data not shown), which is consistent with previous studies (13, 14). In addition, Ratovitski *et al.* (36) have reported that H46R has longer half-life than other FALS mutant SODs in cells by 35-S pulse-chase. We have also obtained similar results that the half-lives of A4V, G37R, and G93A were shorter than H46R (data not shown). Therefore, Fig. 1 suggests that FALS mutant SODs have the propensity to be degraded in the proteasome and that H46R is longer lived than other FALS mutant SODs in cells.

Typical FALS Mutant SODs Are Barely Detected by Monoclonal Antibodies in Western Blot Analyses—We used monoclonal antibodies against human Cu/Zn-SOD (mAbs N6 and SD-G6) to detect expressed human Cu/Zn-SOD proteins in the cell lysate 24 h after transfection. As shown in Fig. 2*A*, WT and C111S were detected by both mAbs, and H46R was detected by mAb N6 slightly. However, A4V, G37R, and G93A were not detected by both mAbs (Fig. 2*A*), even though all proteins were detected at the same level by a polyclonal antibody (Fig. 1, *24 h*).

To analyze further in detail the lowered reactivity of the FALS mutant proteins with these mAbs, purified Cu/Zn-SOD proteins were subjected to Western blot analyses. As shown in Fig. 2*B*, typical FALS mutant SODs, A4V, G37R, and G93A, were scarcely detected by these mAbs, as well as by a third monoclonal antibody, mAb 5c-10. In contrast, H46R was detected by all mAbs to a greater extent than the other FALS mutant SODs, and C111S and WT reacted much more strongly with all mAbs. Each of the nitrocellulose membranes after

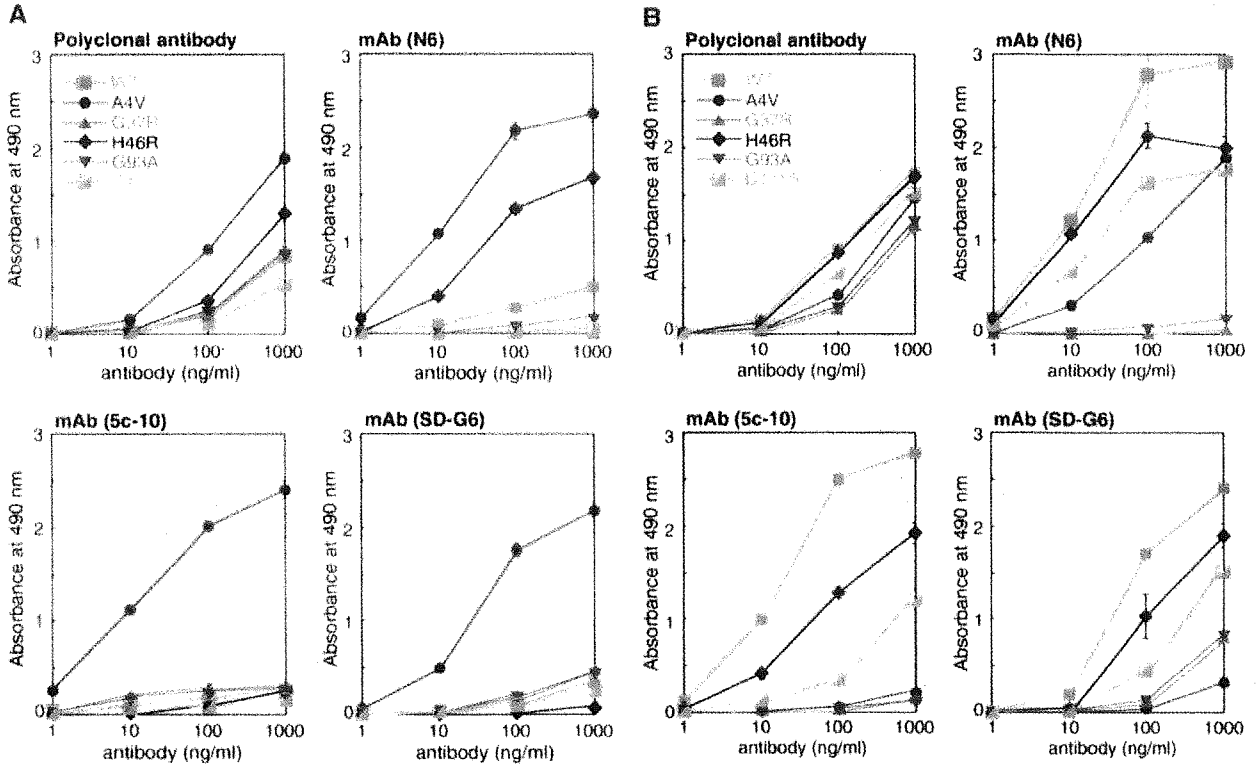

FIG. 3. **ELISA for native SODs and SODs treated the same way as in Western blot analyses.** Purified wild-type and mutant SODs with and without denaturing treatments were diluted to 1 μg/ml in coating buffer (50 mM sodium bicarbonate, pH 9.6). 100 μl of the samples were added to each well of 96-well microplates. The proteins were detected by various concentrations of mAbs and a polyclonal antibody. Data are presented as the means ± S.D. of triplicate experiments. *A*, ELISA for native wild-type and mutant SODs. *B*, ELISA for wild-type and mutant SODs treated the same way as in Western blot analyses.

reacting with the mAbs was de-probed by treatment with a stripping buffer (80 mM Tris-HCl, pH 6.8, containing 2.5% SDS, 1% 2-ME) and re-incubated with a polyclonal antibody. Representative results show that the same amounts of Cu/Zn-SOD proteins are present on the membrane. These results clearly show that typical FALS mutant SODs are barely recognized by the monoclonal antibodies in Western blot analyses despite having only one amino acid replacement.

ELISA for Denatured SODs Showed Results Similar to Western Blotting, although ELISA for Native SODs Did Not—We next examined the reactivity of the purified Cu/Zn-SOD proteins with these mAbs by means of ELISA. Unexpectedly, mAbs 5c-10 and SD-G6 recognized native A4V much stronger than other proteins, and mAb N6 recognized native A4V and H46R strongly (Fig. 3*A*), which is inconsistent with the Western blot results. Thus we performed ELISA for proteins after the treatments in the same manner in Western blotting. The SOD proteins were boiled with 2% 2-ME and 2% SDS for 5 min, diluted with coating buffer (50 mM $NaHCO_3$, pH 9.6) by 200-fold, and then subjected to ELISA. As shown in Fig. 3*B*, the treated WT, H46R, and C111S reacted with all the mAbs much more strongly than typical FALS mutant SODs. The reactivity of A4V to these mAbs was drastically decreased by this treatment. All of the treated proteins had almost the same reactivity with the polyclonal antibody. These results were very similar to the results obtained in the Western blot analyses.

All Epitopes of mAbs N6, 5c-10, and SD-G6 Are Located in the Greek Key Loop VI—The question arises as to which region of the human Cu/Zn-SOD is recognized by these monoclonal antibodies. Because there is no map of their epitopes, we performed epitope mapping for these mAbs, N6, 5c-10, and SD-G6. WT was digested with lysyl endopeptidase, and the digest was fractionated by HPLC on a Sephacryl C18 column (Fig. 4*A*). Although three peptides, 1–3, 4–9, and 129–136 were lost, the peptides corresponding to nine peaks from 1 to 9 were identified as residues 71–75, 123–128, 24–30, 76–91, 71–91, 31–36, and137–153, a mixture of 10–23, 37–70, and 92–122, respectively, as shown in Fig. 4*B*, by amino acid sequencing and mass spectrometry analyses. These peptides were diluted 10-fold with PBS(−) and subjected to ELISA. Only one peptide in peak 9, which corresponds to residues 92–122, reacted with all the mAbs (Fig. 4*C*). On the other hand, the polyclonal antibody reacted with peptides in peaks 5 and 7–9. The ELISA of peptides from digested A4V also showed the same results. To further identify the epitope for each mAb, the synthesized peptides were subjected to ELISA. As shown in Fig. 4*D* (*a* and *b*), peptide 102–116 reacted strongly with all the mAbs and the polyclonal antibody. Moreover, because residues 102–114 and 103–116 did not react with all the mAbs and the polyclonal antibody (Fig. 4*D* (*c*)), we conclude that epitopes of these mAbs are located within residues 102–115. These results clearly indicate that Ser-102 and Arg-115 are essential for binding to all the mAbs and the polyclonal antibody. Epitopes of the mAbs and polyclonal antibody may be composed of Ser-102 and Arg-115 and some residues between Val-103 and Gly-114. The residues 102–115 corresponds to Greek key loop VI between β-sheet 4f (residues 94–101) and β-sheet 7g (residues 116–120) in the tertiary structure of human Cu/Zn-SOD (Fig. 4*E*, *red line*). It is interesting to note that the epitopes of all mAbs are located in the same region even though they were obtained from different sources, suggesting that this loop may be a strong antigenic region in Cu/Zn-SOD. However, epitopes of the three mAbs are not identical and have different characters. N6 reacts with native A4V and H46R strongly

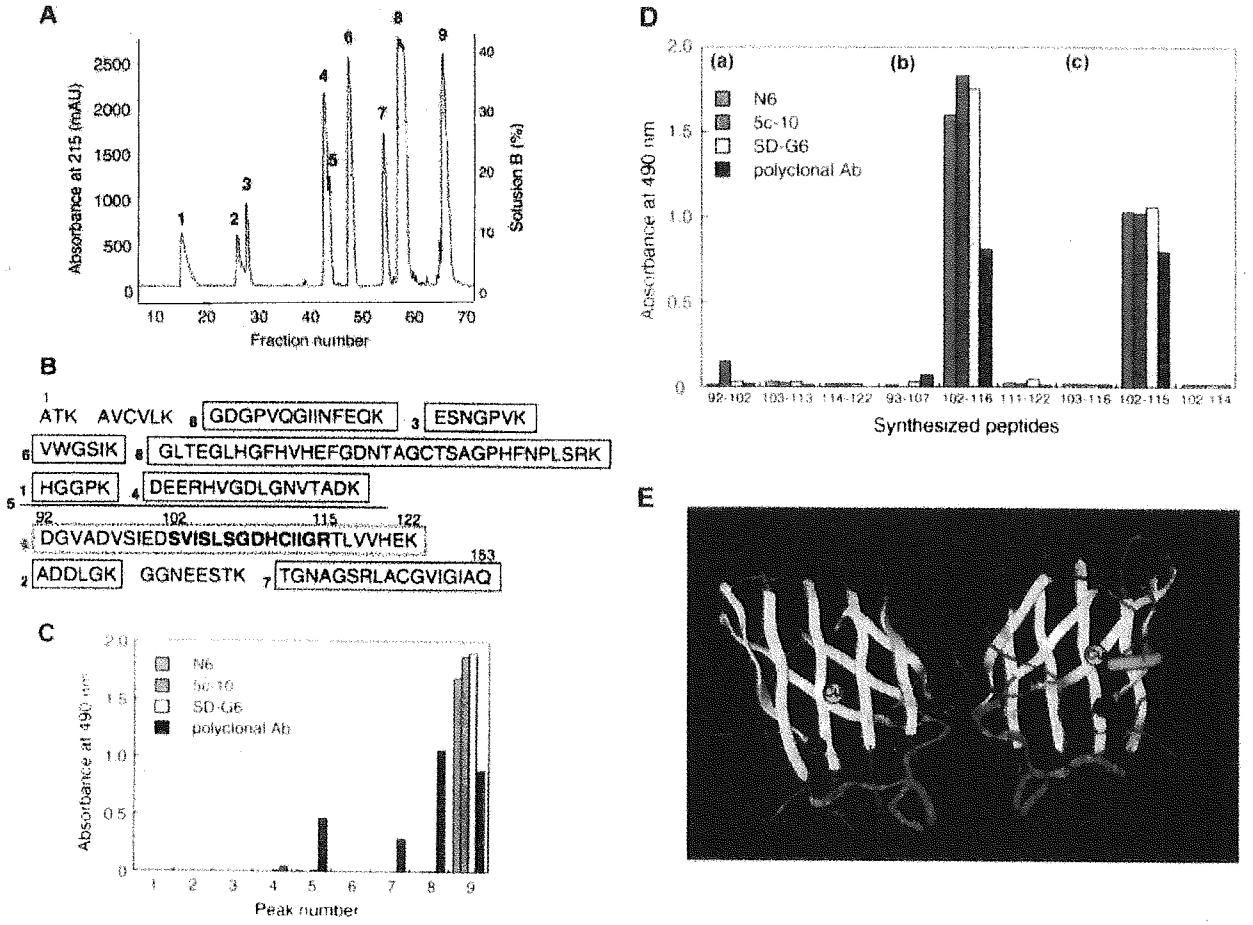

FIG. 4. **Epitope mapping of monoclonal antibodies.** *A*, wild-type SOD was digested with lysyl endopeptidase, and the digest was fractionated by HPLC using a Sephacryl C18 column. *B*, peptide mapping of human Cu/Zn-SOD. *Numbers beside* the *boxes* and *numbers above* the *amino acids* show the peak number in *A* and amino acid residue number, respectively. *C*, ELISA for the separated peptides. *D*, ELISA for synthesized peptides. Peak 9 (92–122) was divided into three peptides. *a*, each peptide consists of 11 or 9 amino acids. *b*, each peptide consists of 15 or 12 amino acids. *c*, peptides from which one or two amino acids were deleted (102–116) (*b*). *E*, epitope of the mAbs was indicated as *red lines* on the tertiary structure of A4V Cu/Zn-SOD (Protein Data Bank code 1N19).

(Fig. 3*A*) and does not react with native and denatured G37R well (Figs. 5–7), even at higher concentrations (data not shown). 5c-10 and SD-G6 recognize native A4V much stronger than other mutant SODs (Fig. 3*A*) and does not react with native H46R well.

DTT Treatment Causes Clear Differences in Immunoreactivity against mAbs between Wild-type-like Proteins and FALS Mutant Cu/Zn-SOD Proteins—Because SDS-PAGE and Western blot analyses includes a reduction with 2-ME, denaturation with SDS, and heating, we investigated the influence of each unfolding treatment on the immunoreactivity of these SOD proteins against mAbs. These SOD proteins were first treated with various concentrations of DTT in the coating buffer for 40 min and then subjected to ELISA. As shown in Fig. 5, the immunoreactivities of A4V, G37R, and G93A against all mAbs decreased after treatment with DTT at concentrations above 1 mM. On the other hand, the immunoreactivities of WT, C111S, and H46R toward all the mAbs increased at the same concentration of DTT. These data suggest that the denaturation by DTT causes clear opposite tendencies between typical FALS mutant SODs (A4V, G37R, and G93A) and wild-type like proteins (WT, C111S, and H46R), and may contribute to the differences of the recognition by mAbs in Western blot analyses. The rationale for including H46R in this group is described under the "Discussion."

SDS Treatment Affects the Immunoreactivity of SODs against mAbs—The effect of SDS treatment on reactivity against the mAbs was also monitored. SOD proteins were treated with various concentrations of SDS for 40 min, diluted 200-fold with the coating buffer, and then subjected to ELISA. As shown in Fig. 6, the immunoreactivity of both WT and mutant proteins against mAb 5c-10 and mAb SD-G6 decreased after incubation with 0.01–0.1% SDS. The reactivity of WT, C111S against 5c-10 increased only after incubation with 2% SDS. On the other hand, the reactivity of WT, C111S, and H46R against mAb N6 was increased after incubation with 1–2% SDS, whereas the reactivity of the typical FALS mutants (A4V, G37R, and G93A) decreased against all the mAbs in an SDS concentration-dependent manner.

Heat Treatment also Affects the Immunoreactivity of SODs against mAbs—Finally, the SOD proteins were incubated at various temperatures in coating buffer for 5 min by using thermal circler (Takara Bio), diluted 200-fold with the coating buffer, and then subjected to ELISA. As shown in Fig. 7, the immunoreactivity of FALS mutant SODs toward all mAbs decreased with increasing treatment temperature until 70 °C. However, the reactivity of WT and C111S against mAb N6 was drastically increased at 80 and 90 °C, respectively. The reactivity of H46R against N6 but not 5c-10 or SD-G6 was also maintained at higher temperatures. The reactivity

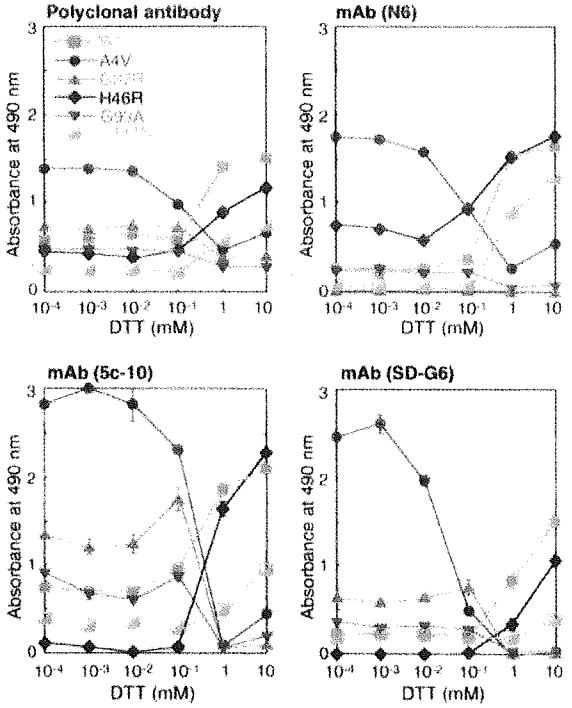

FIG. 5. **Effects of DTT treatment on immunoreactivities of the SODs to monoclonal and polyclonal antibodies.** Purified wild-type and mutant SODs were treated with various concentrations of DTT for 40 min at room temperature and diluted to 1 μg/ml in coating buffer (50 mM sodium bicarbonate, pH 9.6). 100 ng of proteins were coated on an ELISA plate and reacted with the monoclonal or polyclonal antibodies indicated in the figures. Data are presented as the means ± S.D. of triplicate experiments.

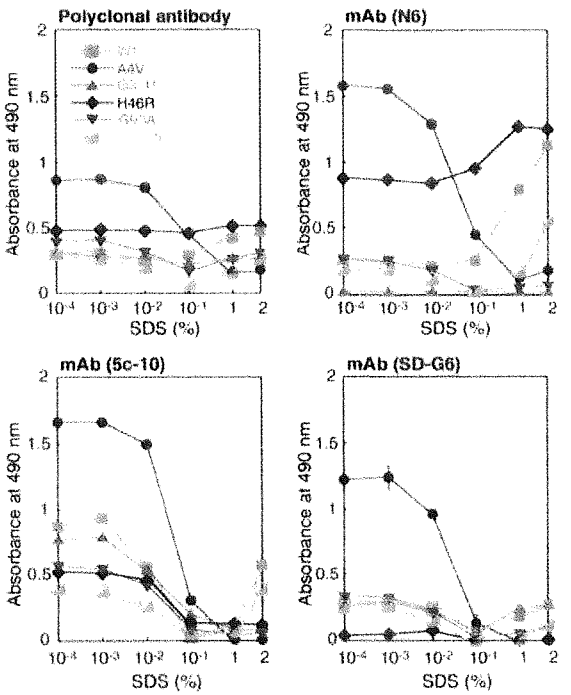

FIG. 6. **Effects of SDS treatment on immunoreactivities of the SODs to monoclonal and polyclonal antibodies.** Purified wild-type and mutant SODs were treated with various concentrations of SDS for 40 min at room temperature and diluted to 1 μg/ml in the coating buffer. 100 ng of proteins were coated into the ELISA plate and were reacted with monoclonal or polyclonal antibodies indicated in the figures. Data are presented as the means ± S.D. of triplicate experiments.

of all the SODs against SD-G6 decreased with increasing treatment temperature.

The Different Immunorecognition by mAbs between Wild-type and FALS Mutant SODs Is Not Due to a Different Binding Efficiency to ELISA Plate—A question may arise as to whether the different recognition by mAbs on ELISA (Figs. 5–7) is because of a differential coating efficiency between WT and mutant SODs on the ELISA plate or a different mAbs recognition itself. However, the protein levels on the plate were too low to be measured by authentic protein assay. Stable dinitrophenylated (DNP) protein is easily obtained by incubation with DNBS in alkaline pH solution (32). Because Picotan/picotein rabbit anti-DNP can react with the DNP proteins of the order of picogram, but not free DNP, we used this system to examine the coating efficiency. Purified SODs were treated with DNBS, diluted to various concentrations (0.05–1 μg/ml) in coating buffer, and coated on the ELISA plates. As shown in Fig. 8*A*, Picotan/picotein rabbit anti-DNP detected all DNP-SODs in the same degree, although the reaction with DNP-C111S was slightly lower. On the other hand, mAb N6 reacted with DNP-C111S strongly and with DNP-WT and DNP-A4V moderately (Fig. 8*B*), even though mAb N6 recognized native A4V and H46R strongly (Fig. 3*A*). To examine further whether the dinitrophenylation of SODs affects the immunorecognition by mAb N6 or not, SODs were treated with the same conditions in the absence of DNBS and detected by mAb N6 (Fig. 8*C*). The similar results in Fig. 8, *B* and *C*, indicate that the dinitrophenylation of SODs does not affect immunoreactivity of mAb N6. The treatment at 37 °C in alkaline solution would lead a partial denaturation of SODs. These data could exclude the possibility that a differential coating efficiency between WT and mutant SODs on the ELISA plate causes the different ELISA signal.

CD Analyses Showed That FALS Mutant SODs, Especially H46R and A4V, Are Susceptible to Denaturation by DTT, SDS, and Heat Treatment—The effects of these unfolding treatments, such as DTT, SDS, and heat treatment, on the secondary (whole) structure of SOD proteins were assessed by CD measurements. The spectra of all of the SODs were almost the same for the native state, although H46R showed a slightly different spectrum (Fig. 9*A*). These SODs, in coating buffer, were reduced with various concentrations of DTT for 40 min and then subjected to CD analysis. 0.1 mM DTT began to induce small denaturation in H46R, A4V, and G93A (Fig. 9*B*), and all the FALS mutant SODs, except WT and C111S, were denatured by 1 mM DTT treatment (Fig. 9*C*). The reduced FALS mutant SODs showed a larger negative band at about 202 nm, an increased negative ellipticity from 220 to 240 nm, and a less negative band in the 215 nm region, which indicates an increased random coil/unordered structure and a decreased β-structure.

We next examined the effect of SDS on the structure of these proteins. As shown in Fig. 9*D*, treatment with 2% SDS caused a loss of secondary structure in only H46R and A4V but not in WT, C111S, G37R, and G93A. The structure of H46R and A4V began to change by treatment with SDS at concentrations above 0.05% (data not shown). The CD profiles showed more helical conformation as reported for monomeric *Escherichia coli* Cu/Zn-SOD treated with SDS at concentrations above 10% (37), which are quite different from the form produced by reduction with DTT (Fig. 9*C*). These data indicate that only H46R and A4V are quite sensitive to SDS and that a propensity toward denaturation by SDS is not common among FALS mutant SODs.

Finally, all SODs that were boiled in the coating buffer for 5 min were subjected to CD analyses. As shown in Fig. 9*E*, the

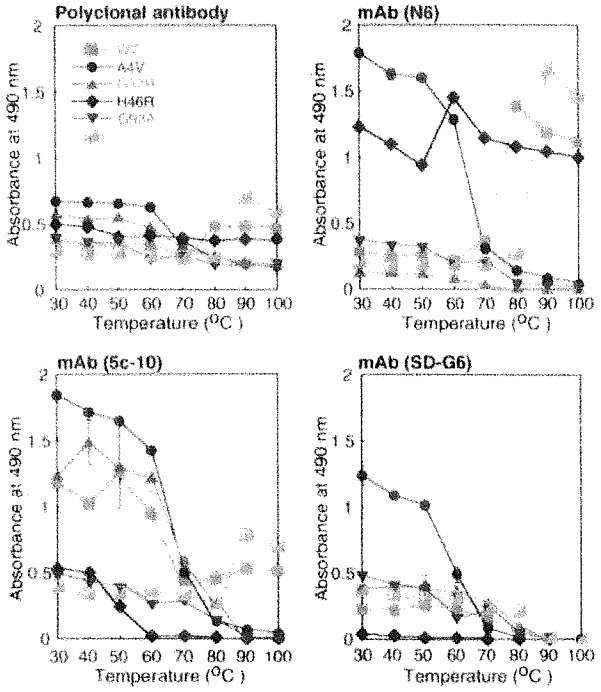

FIG. 7. **Effects of heating on immunoreactivities of the SODs to monoclonal and polyclonal antibodies.** Purified wild-type and mutant SODs were treated at various temperatures for 5 min and diluted to 1 μg/ml with coating buffer. 100 ng of proteins were coated into ELISA plate and reacted with monoclonal or polyclonal antibodies indicated in the figures. Data are presented as the means ± S.D. of triplicate experiments.

CD spectra of all proteins were identical, even though differences in immunoreactivity between wild-type SOD and FALS mutant SODs, when treated at over 80 or 90 °C, were detected by ELISA for mAb N6 and mAb 5c-10 (Fig. 7). Because the CD spectra patterns also showed lower ellipticity from 220 to 240 nm as well as the reduced FALS mutant SODs (Fig. 9*C*), we monitored the transition curves of these proteins at 25–70 °C at a wavelength of 230 nm. H46R and A4V began to denature at a lower temperature, indicating that both are much more thermolabile than the other SODs (Fig. 9*F*). These results indicate that FALS mutant SODs, especially H46R and A4V, are susceptible to denaturation by DTT, SDS, and heat treatment.

DISCUSSION

Although there is some evidence to show that the FALS mutant SODs have a toxic gain of function, the mechanism responsible of this pathology is unknown. Finding the differences of properties between wild-type and FALS mutant SODs and the common characteristics of FALS mutant SODs will give clues to solve the etiology of FALS. The findings here show that typical FALS mutant SODs, but not wild-type SOD, are barely recognized by three monoclonal antibodies in Western blot analyses and ELISA after denaturation, which were in parallel with their degree of increased biological turnover of FALS mutants. Because the epitopes of the three mAbs were mapped within residues 102–115 (Greek key loop VI), variations in recognition by the mAbs may indicate different conformations in this loop. We have observed that the conformation of the peptide 92–122 (Fig. 4*C*, *peak 9*), including the Greek key loop VI, is changeable depending on the solvents, such as water, saline (150 mM NaCl), and PBS, by CD measurements and that the peptide reacts with mAb N6 only when solved in PBS on ELISA.[2] Preliminary one-dimensional ^{1}H NMR spectroscopy of the peptide 92–122 was also performed by a Bruker DRX-800 spectrometer. Most of the NMR peaks derived from the aromatic and amide ^{1}H spins were observed in a narrow spectra range from 7.9 to 8.7 ppm. In addition, peaks from the aliphatic spins were crowded and were separated into several groups. These features of the ^{1}H spectra also suggest that the peptide 92–122 takes neither a typical secondary structure nor a rigid conformation.[3]

Shipp *et al.* (38) have reported that comparison of dynamic properties between G93A and wild-type by NMR spectroscopy showed that G93A exhibits a higher mobility than wild type, particularly in loop III (residues 37–40), which is another short Greek key loop, and loop V (residues 89–93). The increased mobility of the longer Greek key loop VI (residues 102–115) was not described in the NMR study. However, Greek key loop VI may also have property to move easily, because loop regions normally display greater mobility than residues involved in secondary structural elements (38). Because the NMR study needs enough stability for analyzing all residues of the polypeptide at room temperature, the Greek key loop VI in G93A may be stable at the native state. On the other hand, the NMR study of A4V failed because degradation was found from the NMR spectra just a few days after purification (38).

The Greek key loop VI contributes to the stability of Cu/Zn-SOD. In particular, Leu-106 and Ile-113 in the Greek key loop act to stabilize the β-barrel and dimer interface. The Leu-106 side chain points toward the protein core to create a "cork," which stabilizes the β-barrel structure through hydrophobic interactions (39). The mutation from Cys-111 to Ser-111 (C111S) has an increased conformational stability resulting, in part, from the stronger side chain to main chain hydrogen bonds from the O^γ of Ser-111 to the N of Ile-113 and the O of Leu-106 in the Greek key loop (10). By contrast, the crystallographic structure of A4V showed that a mutation from Ala-4 to Val-4 causes the movement of the Leu-106 to cork out of the barrel, even though this A4V protein has the mutation from Cys-111 to Ser-111 (40). The higher immunoreactivity of the mAbs against native A4V may indicate this loose shape of the Greek key loop VI. In the case of WT or C111S, the loop may change to the loose shape only after denaturation. Further studies on which shape of the Greek key loop VI reacts with each mAb will be needed.

Reduction by DTT caused the largest differences in recognition by mAbs between wild-type and FALS mutant SODs. As shown in Fig. 5, the immunoreactivities of A4V, G37R, and G93A against all mAbs were drastically decreased when treated with DTT at concentrations above 1 mM, whereas those of WT, C111S, and H46R increased oppositely at the same concentration of DTT. CD analyses also showed that FALS mutant SODs are much more unstable to DTT treatment than WT and C111S (Fig. 9*C*). Tiwari and Hayword (41) reported that, in the presence of disulfide-reducing agents, FALS mutant SODs were more susceptible than WT to aberrant migration during partially denaturing SDS-PAGE and to proteolytic digestion. A conserved internal disulfide bond between Cys-57 and Cys-146 also contributes to the stability of Cu/Zn-SOD. Cys-57 is located in the longest loop IV containing residues 49–84 between β-sheet 6d and β-sheet 5e, which comprises part of the dimer interface and forms the zinc-binding site. Cys-146 is located in β-sheet 8h containing residues 145–152. A part in the β-sheet 8h is hydrogen bonding with Gly-114 and Arg-115 in the Greek key loop VI (9). Therefore, the presence of DTT in coating buffer, pH 9.6, would induce the cleavage of the

[3] T. Ikegami and N. Fujiwara, unpublished data.

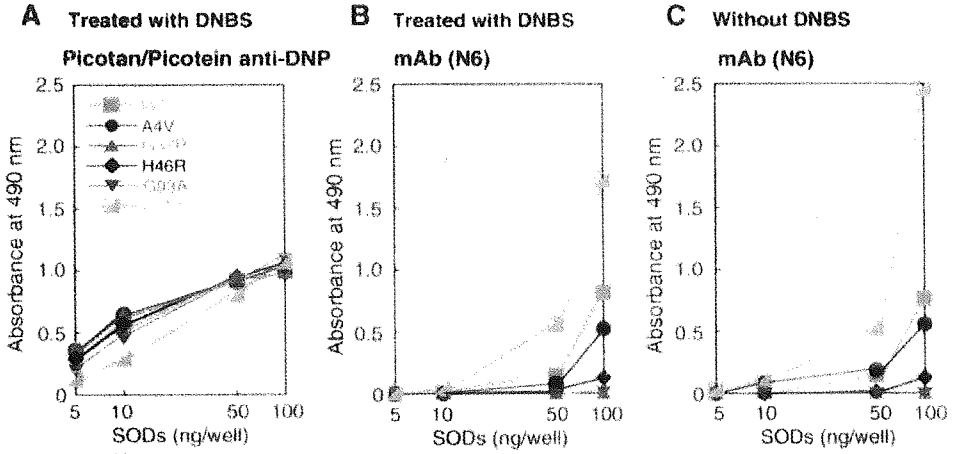

FIG. 8. **Determination of coating efficiency of wild-type and mutant SODs to ELISA plate by using DNP-SODs and Picotan/picotein rabbit anti-DNP.** DNP-SODs were coated on the ELISA plate and reacted with Picotan/picotein rabbit anti-DNP (*A*) and with mAb N6 (*B*). *C*, SODs were treated with the same conditions of dinitrophenylation in the absence of DNBS and detected by mAb N6. Data are presented as the means ± S.D. of triplicate experiments.

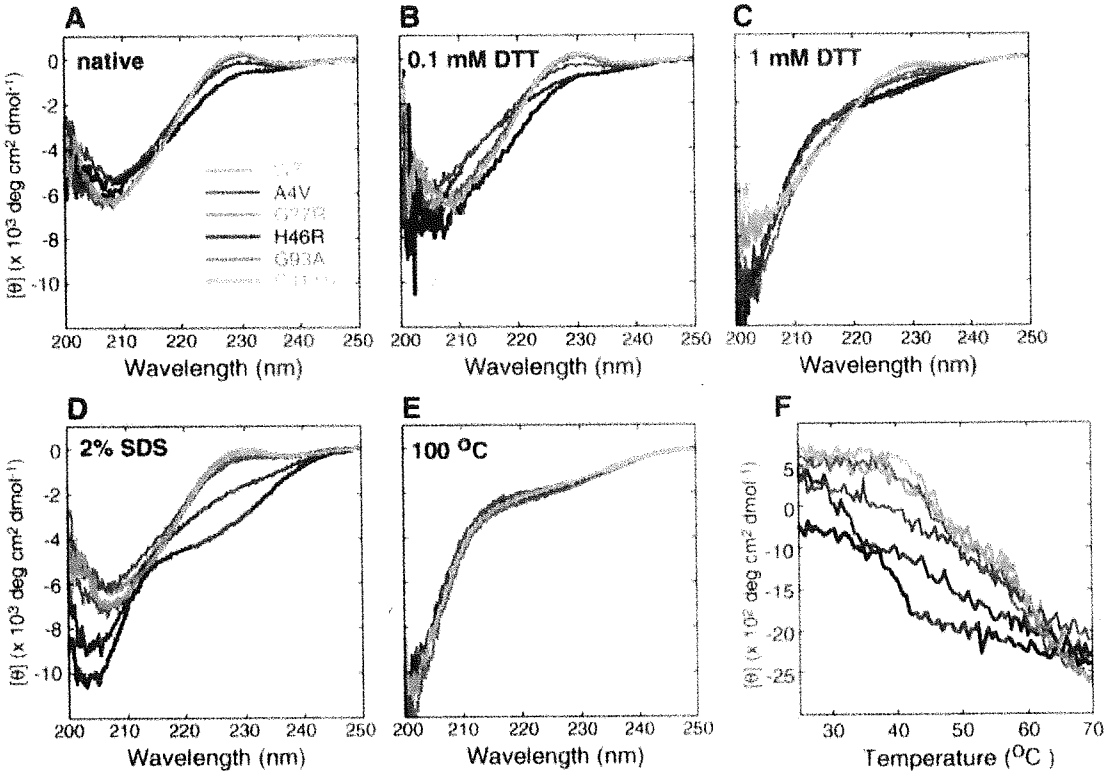

FIG. 9. **Effects of DTT, SDS, and heating on far-UV CD spectra of the Cu/Zn-SOD proteins.** *A*, CD spectra of native wild-type and mutant SODs in coating buffer. *B*, CD spectra of wild-type and mutant SODs treated with 0.1 mM DTT in coating buffer for 40 min. *C*, CD spectra of wild-type and mutant SODs treated with 1 mM DTT in coating buffer for 40 min. *D*, CD spectra of wild-type and mutant SODs treated with 2% SDS in coating buffer for 40 min. *E*, CD spectra of wild-type and mutant SODs boiled in coating buffer for 5 min. *F*, transitions in the CD ellipticities of wild-type and mutant SODs at 25–70 °C monitored at a wavelength of 230 nm.

disulfide bond and cause disorder in loop IV, the β-sheet 8h, and the structure of the Greek key loop VI. However, even though the mutation sites are far from the Greek key loop VI and each mutation site is different, the question of why it is clearly different in terms of immunoreactivity against mAbs between wild-type Cu/Zn-SOD-like proteins (WT, C111S, and H46R) and typical FALS mutant SODs (A4V, G37R, and G93A) after DTT treatment remains unanswered. The reason for why H46R is included in the wild-type like SOD group is discussed below.

Because His-46 is one of the copper-ligand amino acids in Cu/Zn-SOD, the mutant enzyme, H46R, contains no copper and thus is SOD-inactive (4). However, the possibility must be considered that H46R is more stable than other typical FALS mutant SODs. Among FALS patients, the clinical progression is quite different from the mutations in the *SOD1* gene. For H46R patients, the progression is extremely slow, with a mean survival of 16.8 years (42). In contrast, the mean survival of G93A cases in one report was 2.2 years (43). Recently, Nagai *et*

al. (44) established an H46R rat and a G93A rat. Even though the H46R SOD protein level in the H46R rat was much higher than that in the G93A rat, both the onset and the rate of progression of the disease in the H46R rat were much slower than those for the G93A rat (44). We also observed that H46R has a longer half-life than the other FALS mutants (Fig. 1) (36). Moreover, Niwa *et al.* (15) reported that ubiquitination of H46R by Dorfin, which is the likely ubiquitin ligase for FALS mutant SODs, was lower than other FALS mutant SODs. Recently, Miyazaki *et al.* (45) reported that NEDL1, a novel HECT-type ubiquitin ligase, also ubiquitinates FALS mutants and that the degree of ubiquitination of mutant SODs was dependent on the disease severity of FALS (A4V > G93A > H46R). These results also indicate that H46R is much more stable than other FALS mutant SODs *in vivo*. In contrast, the recombinant H46R protein is quite sensitive to DTT, SDS, and heat treatment (Fig. 9). Several papers (41, 46) have also reported that H46R is less stable than other FALS mutants *in vitro*. Most interestingly, the immunoreactivities of H46R against the mAbs in Western blot and ELISA were similar to that of WT or C111S (Figs. 2, 3, and 5–7). Therefore, local conformational changes monitored with mAbs will be useful for understanding the discrepancy between the instability of the H46R protein *in vitro* and the slower clinical progression of H46R patients.

There is accumulating evidence that FALS mutant SODs also tend to form aggregates under the destabilizing conditions (19–22), similar to other neurodegenerative disorders such as Alzheimer's, Parkinson's, Huntington's, and prion diseases. It is generally thought that aggregation or amyloid formation requires a conformational transition in a polypeptide chain from a native form to a mis-folded conformation in these diseases. In the case of prion disease, the conformational conversion of a normal α-helical rich cellular prion protein (PrP^c) to an abnormal and insoluble β-sheet rich form (PrP^{sc}) is a key event in the pathogenesis (47). The structural rearrangement in the central portion (residues 90–120) in the PrP^c is associated with the conversion to the infectious conformer (25). Thus the peculiar, subtle conformational change in the Greek key loop in FALS mutant SODs may also serve as a trigger for aggregation or amyloid formation. Moreover, if small change in FALS mutant SODs are recognized by ubiquitin ligase specific for FALS mutant SOD proteins, such as Dorfin or NEDL1, FALS mutant SODs would undergo a more rapid degradation in cells. To determine the significance of the alteration in the Greek key loop for FALS mutant SODs, further studies using various mAbs recognizing other regions and other mutant SODs are needed.

In the present study, we found different recognition by mAbs between wild-type and FALS mutant SODs under the denatured conditions, which suggests that different conformations are induced around the Greek key loop during the unfolding process. This new approach using mAbs will contribute to a better understanding of the molecular mechanism of the conformational perturbation of FALS mutant proteins, and may be of value in the development of a diagnosis and therapeutic agents for use in treating FALS.

Acknowledgments—We thank Dr. Taizou Uda (Hiroshima Prefecture University) for kindly providing mAb 5c-10. We are grateful to Dr. Tomitake Tsukihara (Institute of Protein Research, Osaka University) for helpful comments.

REFERENCES

1. Deng, H. X., Hentati, A., Tainer, J. A., Zafar, I., Cayabyab, A., Hung, W. Y., Getzoff, E. D., Hu, P., Herzfeldt, B., Roos, R. P., Warner, C., Deng, G., Soriano, E., Smyth, C., Parge, H. E., Ahmed, A., Roses, A. D., Hallewell, R. A., Pericak-Vance, M. A., and Siddique, T. (1993) *Science* **261,** 1047–1051
2. Rosen, D. R., Siddique, T., Patterson, D., Figlewicz, D. A., Sapp, P., Hentati, A., Donaldson, D., Goto, J., O'Regan, J. P., Deng, H. X., Rahmani, Z., Krizus, A., McKenna-Yasek, D., Cayabyab, A., Gaston, S. M., Berger, R., Tanzi, R. E., Halperin, J. J., Herzfeldt, B., Van den Bergh, R., Hung, W. Y., Bird, T., Deng, G., Mulder, D. W., Smyth, C., Laing, N. G., Soriano, E., Pericak-Vance, M. A., Hains, J., Rouleau, G. A., Gusella, J. S., Horvitz, H. R., and Brown, R. H., Jr. (1993) *Nature* **362,** 59–62
3. Valentine, J. S., and Hart, P. J. (2003) *Proc. Natl. Acad. Sci. U. S. A.* **100,** 3617–3622
4. Okado-Matsumoto, A., Myint, T., Fujii, J., and Taniguchi, N. (2002) *Free Radic. Res.* **33,** 65–73
5. Gurney, M. E., Pu, H., Chiu, A. Y., Dal Canto, M. C., Polchow, C. Y., Alexander, D. D., Caliendo, J., Hentati, A., Kwon, Y. W., Deng, H. X., Chen, W., Zhai, P., Sufit, R. L., and Siddique, T. (1994) *Science* **264,** 1772–1775
6. Ripps, M. E., Huntley, G. W., Hof, P. R., Morrison, J. H., and Gordon, J. W. (1995) *Proc. Natl. Acad. Sci. U. S. A.* **92,** 689–693
7. Reaume, A. G., Elliott, J. L., Hoffman, E. K., Kowall, N. W., Ferrante, R. J., Siwek, D. F., Wilcox, H. M., Flood, D. G., Beal, M. F., Brown, R. H., Jr., Scott, R. W., and Snider, W. D. (1996) *Nat. Genet.* **13,** 43–47
8. Julien, J. P. (2001) *Cell* **104,** 581–591
9. Tainer, J. A., Getzoff, E. D., Beem, K. M., Richardson, J. S., and Richardson, D. C. (1982) *J. Mol. Biol.* **160,** 181–217
10. Parge, H. E., Hallewell, R. A., and Tainer, J. A. (1992) *Proc. Natl. Acad. Sci. U. S. A.* **89,** 6109–6113
11. Lindberg, M. J., Tibell, L., and Oliveberg, M. (2002) *Proc. Natl. Acad. Sci. U. S. A.* **99,** 16607–16612
12. Hayward, L. J., Rodriguez, J. A., Kim, J. W., Tiwari, A., Goto, J. J., Cabelli, D. E., Valentine, J. S., and Brown, R. H., Jr. (2002) *J. Biol. Chem.* **277,** 15923–15931
13. Borchelt, D. R., Lee, M. K., Slunt, H. S., Guarnieri, M., Xu, Z. S., Wong, P. C., Brown, R. H., Jr., Price, D. L., Sisodia, S. S., and Cleveland, D. W. (1994) *Proc. Natl. Acad. Sci. U. S. A.* **91,** 8292–8296
14. Hoffman, E. K., Wilcox, H. M., Scott, R. W., and Siman, R. (1996) *J. Neurol. Sci.* **139,** 15–20
15. Niwa, J., Ishigaki, S., Hishikawa, N., Yamamoto, M., Doyu, M., Murata, S., Tanaka, K., Taniguchi, N., and Sobue, G. (2002) *J. Biol. Chem.* **277,** 36793–36798
16. Takamiya, R., Takahashi, M., Myint, T., Park, Y. S., Miyazawa, N., Endo, T., Fujiwara, N., Sakiyama, H., Misonou, Y., Miyamoto, Y., Fujii, J., and Taniguchi, N. (2003) *FASEB J.* **17,** 938–940
17. Bruijn, L. I., Houseweart, M. K., Kato, S., Anderson, K. L., Anderson, S. D., Ohama, E., Reaume, A. G., Scott, R. W., and Cleveland, D. W. (1998) *Science* **281,** 1851–1854
18. Johnston, J. A., Dalton, M. J., Gurney, M. E., and Kopito, R. R. (2000) *Proc. Natl. Acad. Sci. U. S. A.* **97,** 12571–12576
19. Rakhit, R., Cunningham, P., Furtos-Matei, A., Dahan, S., Qi, X. F., Crow, J. P., Cashman, N. R., Kondejewski, L. H., and Chakrabartty, A. (2002) *J. Biol. Chem.* **277,** 46551–47556
20. Stathopulos, P. B., Rumfeldt, J. A., Scholz, G. A., Irani, R. A., Frey, H. E., Hallewell, R. A., Lepock, J. R., and Meiering, E. M. (2003) *Proc. Natl. Acad. Sci. U. S. A.* **100,** 7021–7026
21. DiDonato, M., Craig, L., Huff, M. E., Thayer, M. M., Cardoso, R. M., Kassmann, C. J., Lo, T. P., Bruns, C. K., Powers, E. T., Kelly, J. W., Getzoff, E. D., and Tainer, J. A. (2003) *J. Mol. Biol.* **332,** 601–615
22. Elam, J. S., Taylor, A. B., Strange, R., Antonyuk, S., Doucette, P. A., Rodriguez, J. A., Hasnain, S. S., Hayward, L. J., Valentine, J. S., Yeates, T. O., and Hart, P. J. (2003) *Nat. Struct. Biol.* **10,** 461–467
23. Temussi, P. A., Masino, L., and Pastore, A. (2003) *EMBO J.* **22,** 355–361
24. Peretz, D., Williamson, R. A., Matsunaga, Y., Serban, H., Pinilla, C., Bastidas, R. B., Rozenshteyn, R., James, T. L., Houghten, R. A., Cohen, F. E., Prusiner, S. B., and Burton, D. R. (1997) *J. Mol. Biol.* **273,** 614–622
25. Leclerc, E., Peretz, D., Ball, H., Sakurai, H., Legname, G., Serban, A., Prusiner, S. B., Burton, D. R., and Williamson, R. A. (2001) *EMBO J.* **20,** 1547–1554
26. Leclerc, E., Peretz, D., Ball, H., Solforosi, L., Legname, G., Safar, J., Serban, A., Prusiner, S. B., Burton, D. R., and Williamson, R. A. (2003) *J. Mol. Biol.* **326,** 475–483
27. Matsunaga, Y., Saito, N., Fujii, A., Yokotani, J., Takakura, T., Nishimura, T., Esaki, H., and Yamada, T. (2002) *Biochem. J.* **361,** 547–556
28. Solomon, B., Koppel, R., Hanan, E., and Katzav, T. (1996) *Proc. Natl. Acad. Sci. U. S. A.* **93,** 452–455
29. Peretz, D., Williamson, R. A., Kaneko, K., Vergara, J., Leclerc, E., Schmitt-Ulms, G., Mehlhorn, I. R., Legname, G., Wormald, M. R., Rudd, P. M., Dwek, R. A., Burton, D. R., and Prusiner, S. B. (2001) *Nature* **412,** 739–743
30. Piwnica-Worms, H. (1987) in *Current Protocols in Molecular Biology* (Ausubel, F. M., Brent, R., Kingston, R. E., Moore, D. D., Seidman, J. G., Smith, J. A., and Struhl, K., eds) pp. 16.8.1–16.11.7, Greene/Wiley Interscience, New York
31. Ho, S. N., Hunt, H. D., Horton, R. M., Pullen, J. K., and Pease, L. R. (1989) *Gene* **77,** 51–59
32. Little, J. R., and Eisen, H. N. (1967) in *Methods in Immunology and Immunochemistry* (William, C. A., and Chase, M. W., eds) Vol. 1, pp. 128–133, Academic Press, New York
33. Goto, J. J., Gralla, E. B., Valentine, J. S., and Cabelli, D. E. (1998) *J. Biol. Chem.* **273,** 30104–30109
34. Lepock, J. R., Frey, H. E., and Hallewell, R. A. (1990) *J. Biol. Chem.* **265,** 21612–21618
35. Hallewell, R. A., Imlay, K. C., Lee, P., Fong, N. M., Gallegos, C., Getzoff, E. D., Tainer, J. A., Cabelli, D. E., Tekamp-Olson, P., Mullenbach, G. T., and Cousens, L. S. (1991) *Biochem. Biophys. Res. Commun.* **181,** 474–480
36. Ratovitski, T., Corson, L. B., Strain, J., Wong, P., Cleveland, D. W., Culotta, V. C., and Borchelt, D. R. (1999) *Hum. Mol. Genet.* **8,** 1451–1460
37. Bozzi, M., Battistoni, A., Sette, M., Melino, S., Rotilio, G., and Paci, M. (2001) *Int. J. Biol. Macromol.* **29,** 99–105
38. Shipp, E. L., Cantini, F., Bertini, I., Valentine, J. S., and Banci, L. (2003)

Biochemistry **42,** 1890–1899
39. Getzoff, E. D., Tainer, J. A., Stempien, M. M., Bell, G. I., and Hallewell, R. A. (1989) *Proteins* **5,** 322–336
40. Cardoso, R. M., Thayer, M. M., DiDonato, M., Lo, T. P., Bruns, C. K., Getzoff, E. D., and Tainer, J. A. (2002) *J. Mol. Biol.* **324,** 247–256
41. Tiwari, A., and Hayward, L. J. (2003) *J. Biol. Chem.* **278,** 5984–5992
42. Aoki, M., Ogasawara, M., Matsubara, Y., Narisawa, K., Nakamura, S., Itoyama, Y., and Abe, K. (1993) *Nat. Genet.* **5,** 323–324
43. Cudkowicz, M., McKenna-Yasek, D., Sapp, P., Chin, W., Geller, B., Hayden, D., Horvtiz, H., and Brown, R. (1997) *Ann. Neurol.* **41,** 210–212
44. Nagai, M., Aoki, M., Miyoshi, I., Kato, M., Pasinelli, P., Kasai, N., Brown, R. H., Jr., and Itoyama, Y. (2001) *J. Neurosci.* **21,** 9246–9254
45. Miyazaki, K., Fujita, T., Ozaki, T., Kato, C., Kurose, Y., Sakamoto, M., Kato, S., Goto, T., Itoyama, Y., Aoki, M., and Nakagawara, A. (2004) *J. Biol. Chem.* **279,** 11327–11335
46. Rodriguez, J. A., Valentine, J. S., Eggers, D. K., Roe, J. A., Tiwari, A., Brown, R. H., Jr., and Hayward, L. J. (2002) *J. Biol. Chem.* **277,** 15932–15937
47. Prusiner, S. B. (1998) *Proc. Natl. Acad. Sci. U. S. A.* **95,** 13363–13383

Am J Physiol Cell Physiol 288: C253–C259, 2005.
First published September 29, 2004; doi:10.1152/ajpcell.00014.2004.

Overexpression of mutated Cu,Zn-SOD in neuroblastoma cells results in cytoskeletal change

Rina Takamiya,[1] Motoko Takahashi,[1] Yong Seek Park,[1] Yoshie Tawara,[1] Noriko Fujiwara,[2] Yasuhide Miyamoto,[1] Jianguo Gu,[1] Keiichiro Suzuki,[2] and Naoyuki Taniguchi[1]

[1]*Department of Biochemistry, Osaka University Graduate School of Medicine, Osaka, Japan; and* [2]*Department of Biochemistry, Hyogo College of Medicine, Hyogo, Japan*

Submitted 9 January 2004; accepted in final form 21 September 2004

Takamiya, Rina, Motoko Takahashi, Yong Seek Park, Yoshie Tawara, Noriko Fujiwara, Yasuhide Miyamoto, Jianguo Gu, Keiichiro Suzuki, and Naoyuki Taniguchi. Overexpression of mutated Cu,Zn-SOD in neuroblastoma cells results in cytoskeletal change. *Am J Physiol Cell Physiol* 288: C253–C259, 2005. First published September 29, 2004; doi:10.1152/ajpcell.00014.2004.—Amyotrophic lateral sclerosis (ALS) involves the progressive degeneration of motor neurons in the spinal cord and the motor cortex. It has been shown that 15–20% of patients with familial ALS (FALS) have defects in the *Sod1* gene, which encodes Cu,Zn-superoxide dismutase (SOD). To elucidate the pathological role of mutated Cu,Zn-SOD, we examined the issue of whether mutated Cu,Zn-SOD affects the cell cycle. Mouse neuroblastoma Neuro-2a cells were transfected with human wild-type or mutated (G37R, G93A) Cu,Zn-SOD. Mutated, Cu,Zn-SOD-transfected cells exhibited marked retardation in cell growth and G_2/M arrest. They also displayed lower reactivity to phalloidin, indicating that the cytoskeleton was disrupted. Immunoprecipitation, two-dimensional gel electrophoresis, and Western blot analysis indicated that mutated Cu,Zn-SOD associates with actin. Similar results were obtained by in vitro incubation experiments with purified actin and mutated Cu,Zn-SOD (G93A). These results suggest that mutated Cu,Zn-SOD in FALS causes cytoskeletal changes by associating with actin, which subsequently causes G_2/M arrest and growth retardation.

amyotrophic lateral sclerosis; copper; zinc superoxide dismutase; G_2/M arrest; neurodegenerative disease

AMYOTROPHIC LATERAL SCLEROSIS (ALS) is a neurodegenerative disease characterized by the selective and progressive dysfunction of motor neurons initiated in middle-aged adults (1). The pathology of the disease results from the death of lower motor neurons in the brainstem and spinal cord and upper motor neurons in the cerebral cortex. Approximately 5–10% of ALS cases are familial ALS (FALS), and among FALS cases, 15–20% have been linked to autosomal dominant inheritance of mutations in Cu,Zn-superoxide dismutase (Cu,Zn-SOD) (10, 30). Cu,Zn-SOD functions as an antioxidative enzyme that catalyzes the conversion of $O_2^-\cdot$ to hydrogen peroxide, which is further detoxified by other antioxidant enzymes such as catalase and glutathione peroxidase. More than 100 types of mutations in Cu,Zn-SOD, which comprises 153 amino acids, have been reported to be associated with the FALS (10). Although some FALS-related mutants show reduced enzymatic activities, many retain full activity (26). Furthermore, transgenic mice that have FALS-associated *Sod1* mutations develop FALS-like symptoms despite elevated Cu,Zn-SOD activity, suggesting that the disease is not caused by the loss of normal enzymatic activity (15). Thus the motor neuron dysfunction observed in FALS is generally thought to be due to the newly acquired neurotoxicity of mutant Cu,Zn-SOD. Several hypotheses have been proposed to explain this toxic gain of function of mutated Cu,Zn-SOD in FALS (6, 18, 19, 29). For example, oxidative stress produced by aberrant catalysis (13, 36), abnormal Cu chemistry (26), decreased glutamate metabolism (6), and increased cytoplasmic aggregation (7, 11, 18, 20, 26, 29) have been studied in the setting of mutated Cu,Zn-SOD. However, the precise mechanism of pathogenesis is not understood.

A pathological hallmark of both sporadic and familial ALS involves the abnormal accumulation of cytoskeletal proteins such as neurofilament, tubulin, and actin in the perikaryon and axon of motor neurons (12, 17, 19, 31). Recent studies have reported that these cytoskeletal changes induce slowing of axonal transport in mutated Cu,Zn-SOD transgenic mice (37).

Previous reports demonstrated that the abnormal regulation of mitotic proteins and an aberrant cell cycle have been observed in neurodegenerative diseases, including Alzheimer's disease and ALS. In those studies, it was suggested that cell cycle signaling may affect the neuronal death pathway (25, 33). Thus we hypothesized that the cell cycle might be affected by mutated Cu,Zn-SOD in FALS.

In this study, mouse neuroblastoma cells were transfected with mutated Cu,Zn-SOD. The mutated Cu,Zn-SOD transfectants grew at a much slower rate than the wild-type transfectants or mock transfectants, and G_2/M arrest was observed in the mutant transfectants. As evidenced by confocal microscopy, cytoskeletal destruction occurred in the mutant transfectants. The issue of how mutated Cu,Zn-SOD affected cytoskeletal components was examined.

MATERIALS AND METHODS

Cell culture and transfection. Neuro-2a (N2a) cells, a mouse neuroblastoma cell line, were grown in DMEM (Sigma, St. Louis, MO) supplemented with 10% fetal bovine serum. Mutated Cu,Zn-SOD cDNA, designated G37R and G93A, were constructed using site-directed mutagenesis with a uracil template as described previously (14). The DNA fragments were ligated to a mammalian expression vector, pcDNA3.1/Zeo (Invitrogen, Carlsbad, CA), which was regulated by the cytomegalovirus promoter. The resulting plasmids were transfected into N2a cells using Lipofectamine reagent (Life Technologies/Invitrogen) according to the manufacturer's instruc-

Address for reprint requests and other correspondence: N. Taniguchi, Dept. of Biochemistry, Osaka Univ. Graduate School of Medicine, B1, 2-2 Yamadaoka, Suita, Osaka 565-0871, Japan (E-mail: proftani@biochem.med.osaka-u.ac.jp).

The costs of publication of this article were defrayed in part by the payment of page charges. The article must therefore be hereby marked "*advertisement*" in accordance with 18 U.S.C. Section 1734 solely to indicate this fact.

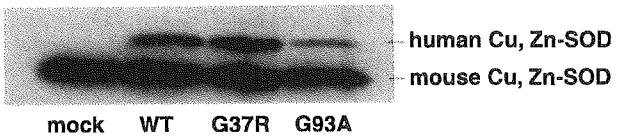

Fig. 1. Characterization of human wild-type and mutated Cu,Zn-superoxide dismutase (SOD) in transfectants of Neuro-2a (N2a) cells, a mouse neuroblastoma cell line. Cell lysates (10 μg) were subjected to 15% SDS-PAGE and subsequent Western blot analysis using an anti-human Cu,Zn-SOD antibody. Mock, mock transfectant; WT, wild-type Cu,Zn-SOD transfectant; G37R, G37R-mutated Cu,Zn-SOD transfectant; G93A, G93A-mutated Cu,Zn-SOD transfectant.

tions. Selection was performed in a medium that contained 1.0 mg/ml Zeocin (GIBCO-BRL/Invitrogen), and, after a 2-wk incubation, several stable colonies were isolated.

Western blot analysis. N2a cells were lysed in buffer [20 mM Tris·HCl, pH 7.4, 150 mM NaCl, 5 mM EDTA, 1% (wt/vol) Nonidet P-40, 1% (wt/vol) Triton, 10% (wt/vol) glycerol, 5 mM sodium pyrophosphate, 10 mM NaF, 1 mM sodium orthovanadate, 10 mM β-glycerophosphate, and 1 mM dithiothreitol (DTT)] with protease inhibitors. Protein (10 μg) was subjected to 15% SDS-PAGE. For Western blot analysis using an anti-Cu,Zn-SOD antibody, the proteins were transferred to nitrocellulose membranes (Schleicher & Schuell, Keene, NH). The blots were blocked with 5% skim milk and 2% BSA and then probed with goat anti-human Cu,Zn-SOD (2). After incubation with a peroxidase-conjugated secondary antibody, immunoreactive bands were visualized using an enhanced chemiluminescence kit (Amersham Biosciences, Piscataway, NJ).

Cell growth curve. Equal numbers (5×10^4) of mock, wild-type, G37R, and G93A Cu,Zn-SOD transfected cells were plated onto six-well tissue culture dishes, and the cell number was determined by hemocytometric counting at 0, 1, 2, and 3 days after cell plating. Triplicate plates were used for each time point (22).

Determination of cell cycle by image analysis. The relative number of cells occupying a particular state of the cell cycle at a specific time was obtained by staining cells with the DNA intercalator propidium iodide (5 μg/ml). Stoichiometric binding resulted when the cells were fixed in cold 70% ethanol for at least 6 h, followed by two washes with PBS and incubation with 100 μg/ml RNase for 30 min at 37°C and two additional washes with PBS (22). Single-parameter histograms were generated by analyzing the cells on a FACStarPlus flow cytometer (BD Biosciences Immunocytometry Systems, San Jose, CA).

Confocal laser scanning microscopy. Cells grown on glass-bottom dishes were fixed with 2% paraformaldehyde-PBS for 10 min on ice. Cells were rinsed in PBS and then treated with 1% saponin for membrane permeabilization. The cells were incubated with 100 ng/ml of tetramethyl rhodamine isothiocyanate (TRITC)-labeled phalloidin (Sigma) or FITC-labeled anti-tubulin antibody (Sigma) for 2 h at room temperature. After washing with PBS with 0.05% Triton five times, the cells were analyzed using confocal laser microscopy. To identify the nuclei, cells were stained with propidium iodide, the size of the nuclei was measured through the microscope, and the image was processed digitally using an eight-bit image analyzer (NIH Image software, version 1.63).

Immunoprecipitation, two-dimensional gel electrophoresis and Western blotting. For the immunoprecipitation of Cu,Zn-SOD or actin, whole cell lysates were incubated with 4 μg of goat anti-human Cu,Zn-SOD antibody or mouse anti-actin antibody (Sigma) and 15 μl of protein G-Sepharose 4 Fast Flow (Amersham Biosciences) for 12 h at 4°C (32). For two-dimensional (2-D) gel electrophoretic analysis, immunoprecipitates were incubated with immobilized pH gradient (IPG) buffer {8 M urea, 2% (wt/vol) 3-([3-cholamidopropyl]dimethylammonio)-2-hydroxy-1-propanesulfonate, 0.5% (vol/vol) carrier ampholyte, pH 3–10, 10 mM DTT, and a trace amount of bromophenol blue} for 4 h. After the samples were centrifuged, the supernatants were subjected to isoelectric focusing using the IPGphor system (Amersham Biosciences) and a 7-cm IPG strip (pH range, 3–10). The IPG strip was then applied to an SDS-PAGE gel (10 or 15%). The gels were subjected to silver staining using the Silver Stain II kit (Daiichi Pure Chemicals, Tokyo, Japan). Western blotting was performed as described above using an anti-Cu,Zn-SOD antibody or an anti-actin antibody.

Purification of Cu,Zn-SOD produced from Sf21 cells. Recombinant Cu,Zn-SOD was isolated from *Spodoptera frugiperda* 21 (Sf21) cells as described previously (34). Briefly, wild-type and mutated Cu,Zn-SOD expression vectors were transfected into Sf21 cells to produce a recombinant virus. For the production of active Cu,Zn-SOD, aqueous solutions of $CuCl_2$ and $ZnCl_2$ were added directly to the medium until reaching a concentration of 1 mM after viral infection. Infected cells ($n = 4 \times 10^8$) were lysed at 4°C in a hypotonic buffer containing 2.5 mM potassium phosphate, pH 7.4, 1 mM benzamidine, and 0.1 mM *p*-amidinophenylmethanesulfonyl fluoride (Wako Pure Chemical Industries, Osaka, Japan). After homogenization and centrifugation at 100,000 *g* for 1 h, the supernatant was subjected to a DE52 ion exchange column chromatography (Whatman, Brentford, UK) in 2.5 mM K^+-phosphate, pH 7.4. Bound proteins were eluted with a linear gradient of K^+-phosphate from 2.5 to 200 mM. To further purify the enzyme, column chromatography was performed on a hydroxyapatite type I column (Bio-Rad, Hercules, CA) with a liner gradient of K^+-phosphate from 10 to 500 mM using Akta Explorer 10s (Amersham Biosciences).

Assay of actin polymerization. An actin polymerization assay was performed in the presence and absence of Cu,Zn-SOD using an Actin Polymerization Biochem kit (Cytoskeleton, Denver, CO) according to the manufacturer's instructions. The samples also were examined by performing immunoprecipitation with anti Cu,Zn-SOD antibody followed by Western blotting using anti-actin antibody.

Statistical evaluation. Differences among mean values were determined by performing one-way ANOVA with Fisher's multiple-comparison test. $P < 0.05$ was considered statistically significant.

RESULTS

Establishment of N2a clones stably expressing wild-type or mutant human Cu,Zn-SOD. N2a cells were stably transfected with wild-type or mutant Cu,Zn-SOD (G37R, G93A), and five

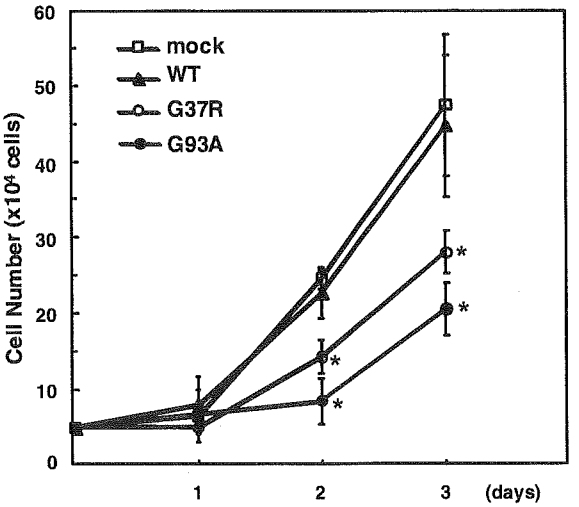

Fig. 2. Growth curves for wild-type or mutated Cu,Zn-SOD-transfected N2a cells. Equal numbers ($n = 5 \times 10^4$ cells) of mock, wild-type, G37R, and G93A Cu,Zn-SOD-transfected cells were plated onto 6-well tissue culture dishes and incubated in DMEM containing 10% FBS. Cell numbers were determined by hemocytometric counting at 0, 1, 2, and 3 days. Each data point is the average of 4 independent experiments. *$P < 0.05$ vs. wild-type Cu,Zn-SOD transfectant.

Zeocin-resistant clones were selected for each cell type. As shown in Fig. 1, the expression levels of Cu,Zn-SOD were verified by Western blot analysis. The upper bands are human enzymes, and the lower bands are endogenous mouse enzymes, as judged by the molecular mass. Because we could not obtain high-expression clones for G93A, the data with indicated clones in Fig. 1 are shown in subsequent figures.

Cell growth arrest in mutant Cu,Zn-SOD-transfected N2a cells. When cell growth was examined, marked inhibition in cell growth was observed in G37R and G93A Cu,Zn-SOD-transfected cells compared with wild-type Cu,Zn-SOD- and mock-transfected cells (Fig. 2). Wild-type Cu,Zn-SOD transfectants showed a growth curve that was similar to that of the mock transfectants. We further determined the cell cycle by conducting flow cytometric analysis. After subconfluent cells were incubated in medium with or without 10% FBS for 48 h, the cells were stained with propidium iodide and subjected to flow cytometric analysis. As shown in Fig. 3*A*, no significant differences were found among mock, wild-type, and mutant Cu,Zn-SOD transfectants in the G_0/G_1 and S phases when grown in a medium containing 10% serum. However, a higher percentage of G37R or G93A Cu,Zn-SOD transfectants was found in the G_2/M phase than with the mock or wild-type Cu,Zn-SOD transfectants. When the cells were subjected to serum starvation, the difference became more obvious; a higher percentage of mock and wild-type Cu,Zn-SOD transfectants was found in the G_0 phase compared with the G37R or G93A Cu,Zn-SOD transfectants, whereas a higher percentage of the mutant transfectants was found in the G_2/M phase compared with mock or wild-type transfectants (Fig. 3*B*). These results suggest that G_2/M arrest occurred with the G37R or G93A Cu,Zn-SOD transfectants.

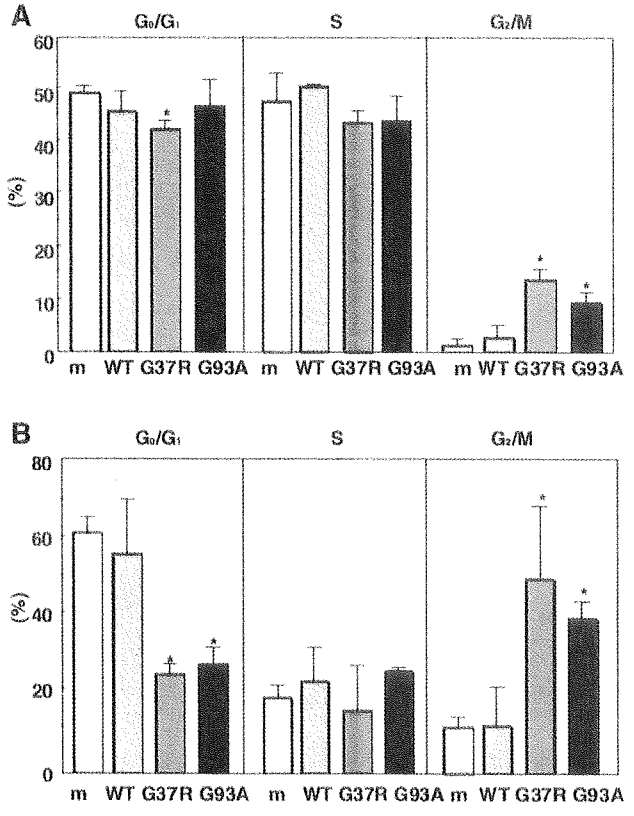

Fig. 3. Cell cycle analysis of wild-type and mutated Cu,Zn-SOD-transfected N2a cells. Cells were incubated in DMEM containing 10% FBS for 1 day and then incubated with or without serum for an additional 48 h. Cell cycles were determined by staining with propidium iodide and by performing flow cytometric analysis. *A*: cells incubated with DMEM containing 10% FBS. *B*: cells were serum starved for 48 h. m, mock transfectant. $^*P < 0.05$ vs. mock transfectant.

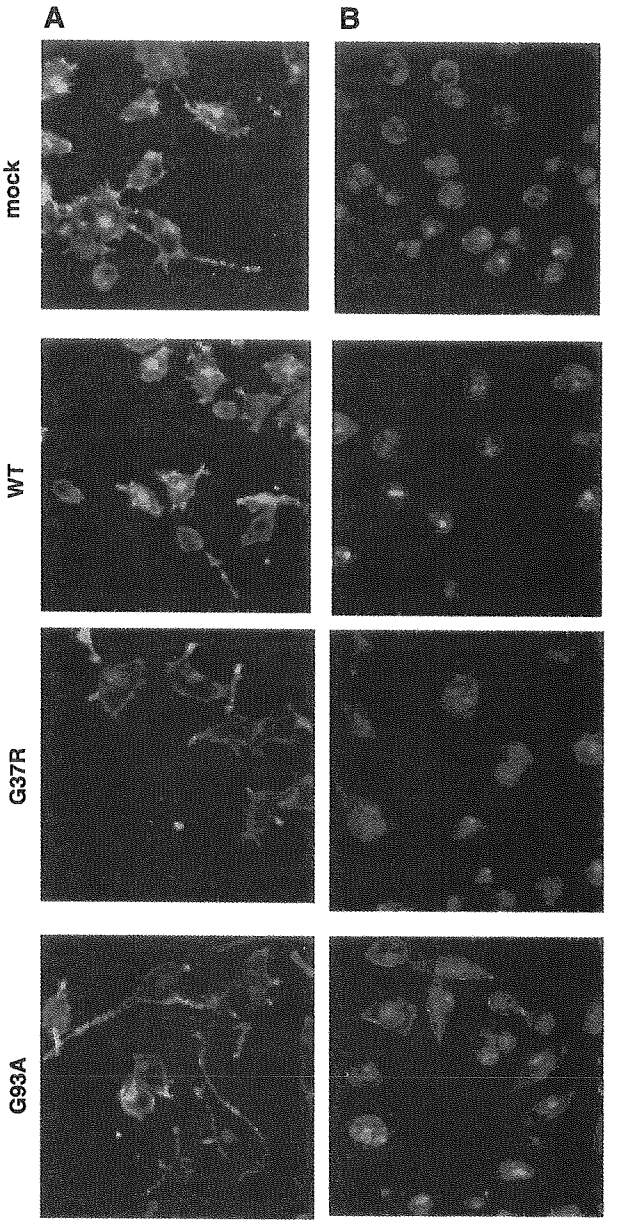

Fig. 4. Determination of cytoskeletal changes in wild-type and mutated Cu,Zn-SOD-transfected N2a cells. After cells were serum starved for 2 days, they were fixed with 2% paraformaldehyde. Florescent images are shown with tetramethylrhodamine isothiocyanate (TRITC)-labeled phalloidin and FITC-labeled anti-α-tubulin antibody. *A*: cells stained with TRITC-labeled phalloidin. *B*: cells stained with FITC-labeled α-tubulin antibody (green) and propidium iodide (red) to identify nuclei. mock, mock transfectant.

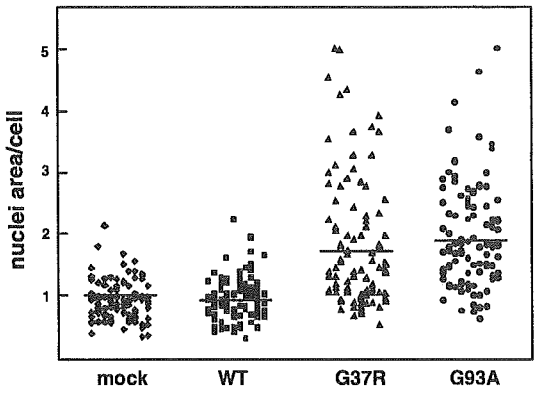

Fig. 5. The size of nuclei in wild-type and mutated Cu,Zn-SOD-transfected N2a cells. After serum starvation for 2 days, the cells were stained with propidium iodide to identify the nucleus. After 100 cells from each culture were randomly collected, the size of the nucleus per cell was measured through the microscope and the image was processed digitally with an 8-bit image analyzer (NIH Image version 1.62). The line in each column indicates the mean value. mock, mock transfectant.

Loss of actin polymerization in mutated, Cu,Zn-SOD-transfected cells. One of the characteristics of the cytoskeletal structure in the M phase is the formation of a contractile ring by actin filaments. The G_2/M arrest observed in mutant transfectants prompted us to examine whether these cells could contain structurally modified actin. After 2-day serum starvation, polymerized actin fiber was stained with phalloidin and analyzed using laser scanning confocal microscopy. As seen in Fig. 4*A*, the G37R or G93A Cu,Zn-SOD transfectants displayed less reactivity to phalloidin than did the mock or wild-type transfectant controls. Such lower reactivity was evident not only in the dendritic processes but also in the cell surface (Fig. 4*A*). This evidence indicates that a decrease in actin polymerization occurred in the mutated Cu,Zn-SOD transfectants. Because tubulin governs the location of the cytoplasm, we next stained the cells with an anti-α-tubulin antibody. As shown in Fig. 4*B*, there were not clarified changes among mock, wild-type, and mutated Cu,Zn-SOD transfectants in α-tubulin immunoreactivities, but some cells with two nuclei were observed in the G93A and G37R Cu,Zn-SOD transfectants. The cells were stained with propidium iodide to determine the area of the nucleus. Fig. 5 indicates the size of the nucleus per cell in each of the transfectants. The mean values of the size of mutant transfectants were almost twice those of wild-type Cu,Zn-SOD or mock transfectants, suggesting that M-phase arrest can occur in mutant-transfected cells.

One of the mutated Cu,Zn-SOD-associated proteins is actin. To examine the changes in cellular protein in the mutant transfectants, 2-D gel electrophoresis was performed. As shown in Fig. 6*A*, significant differences were not found between the wild-type and mutant Cu,Zn-SOD transfectants when a whole cell lysate was examined. However, when the cell lysate was immunoprecipitated with an anti-Cu,Zn-SOD antibody and subjected to 2-D gel electrophoretic analysis, several protein spots with molecular mass of ~40 kDa were found only in mutated Cu,Zn-SOD transfectants as shown in Fig. 6*B*. Because the molecular mass of actin is ~43 kDa, we assumed that one of the spots might be actin. To identify the spots, similarly prepared gels were subjected to Western blot analysis using an anti-actin antibody. Actin-positive spots were observed in the G37R and G93A transfectants but not in the wild-type transfectants (Fig. 7*A*). The samples were next immunoprecipitated with an anti-actin antibody and subjected to Western blot analysis using an anti-Cu,Zn-SOD antibody, the reverse of the former experiment. As shown in Fig. 7*B*, stronger signals were detected in the G37R and G93A Cu,Zn-SOD transfectants than in the wild-type transfectants. These

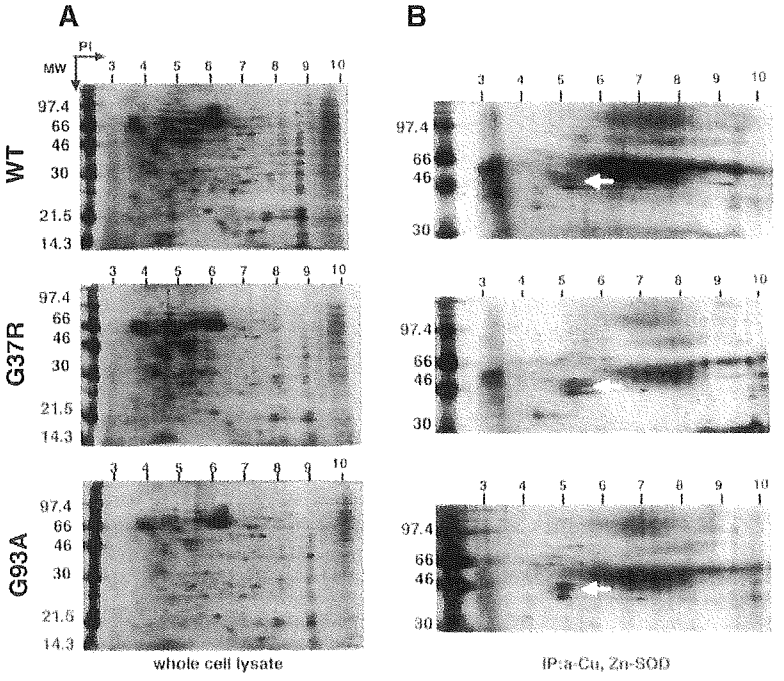

Fig. 6. Two-dimensional (2-D) gel electrophoretic pattern of wild-type and mutated Cu,Zn-SOD-transfected N2a cells. *A*: whole cell lysates (50 μg) of wild-type, G37R, and G93A Cu,Zn-SOD transfectants were subjected to 2-D gel electrophoresis and silver staining. *B*: samples were immunoprecipitated with an anti-Cu,Zn-SOD antibody and subjected to 2-D gel electrophoresis and silver staining.

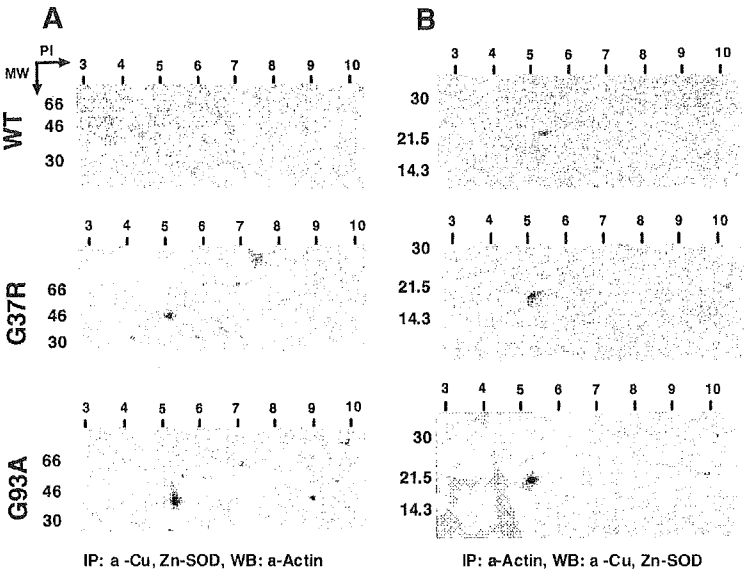

Fig. 7. Determination of Cu,Zn-SOD associated proteins. *A*: samples were immunoprecipitated with an anti-Cu,Zn-SOD antibody and subjected to 2-D gel electrophoresis (10%) and Western blot analysis using an anti-actin antibody. *B*: samples were immunoprecipitated with an anti-actin antibody and subjected to 2-D gel electrophoresis (15%) and Western blot analysis using an anti-Cu,Zn-SOD antibody.

results suggest that mutated Cu,Zn-SOD has a greater tendency to associate with actin protein.

Mutated Cu,Zn-SOD directly associate with actin in vitro. To determine whether mutated Cu,Zn-SOD directly suppressed actin polymerization, we purified wild-type and mutated Cu,Zn-SOD in a baculovirus insect cell system and performed an actin polymerization assay. In this assay, we found that both wild-type and mutated Cu,Zn-SOD did not prevent actin polymerization (data not shown). We then performed in vitro incubation of actin and Cu,Zn-SOD. Actin samples incubated with purified wild-type and mutated Cu,Zn-SOD were immunoprecipitated with anti-Cu,Zn-SOD antibody and subjected to Western blot analysis using an anti-actin antibody. As shown in Fig. 8, a band corresponding to the molecular mass of actin was observed in the mixture with the mutated Cu,Zn-SOD. These results suggest that mutated Cu,Zn-SOD directly associates with actin.

DISCUSSION

Cell cycle changes in mouse neuroblastoma N2a cells transfected with FALS-associated mutants of Cu,Zn-SOD were examined. When G37R and G93A Cu,Zn-SOD mutants were transfected into N2a cells, G_2/M arrest and significant cell growth retardation were observed. Although there were no significant changes in tubulin immunoreactivities, the mutated Cu,Zn-SOD transfectants displayed less reactivity to phalloidin than did the wild-type transfectants, indicating that actin disruption occurred in the mutant transfectants. Immunoprecipitation and 2-D gel electrophoresis followed by Western blot analysis indicated that the mutated Cu,Zn-SOD tended to associate with actin. The in vitro study in which purified Cu,Zn-SOD was incubated with actin indicated that the mutated Cu,Zn-SOD directly associated with actin. G_2/M arrest also occurred in mutated Cu,Zn-SOD-transfected NIH-3T3 cells, although the extent was much less than observed in transfectants of N2a cells (data not shown). Therefore, these phenomena are not considered to be N2a cell specific.

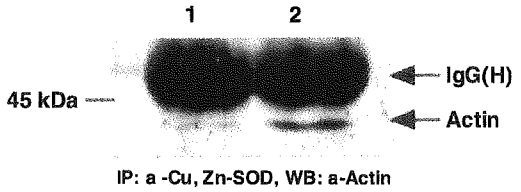

Fig. 8. In vitro association of G93A Cu,Zn-SOD with actin. After wild-type or G93A mutation, Cu,Zn-SOD (0.1 μg) was incubated with human platelet actin (0.1 μg) in actin polymerization buffer (in mM: 50 KCl, 2 $MgCl_2$, and 1 ATP) for 1 h at 24°C, and the samples were immunoprecipitated with an anti-Cu,Zn-SOD antibody and subjected to Western blot analysis using anti-actin antibody. *Lane 1*: wild-type Cu,Zn-SOD incubated with actin; *lane 2*: G93A-mutated Cu,Zn-SOD incubated with actin.

Mutated Cu,Zn-SOD have several enhanced activities that could be capable of selectively damaging interacting proteins or their associated organelles (5, 24, 36, 38). Investigators at our laboratory previously reported that Cu-binding affinities are decreased in mutated Cu,Zn-SOD (26) and mutated Cu,Zn-SOD are highly susceptible to nonenzymatic glycosylation, i.e., glycation (34). It is possible that actin-bound mutated Cu,Zn-SOD is glycated in vivo and reactive oxygen species could be produced via the Fenton reaction involving free Cu ions released from Cu,Zn-SOD (27). Recent reports indicate that hydrogen peroxide causes an increase in F- and G-actin oxidation and a decrease in the F-actin fraction (3, 4). The association of mutated Cu,Zn-SOD with actin might be unexpectedly toxic to the actin cytoskeleton.

Cytoskeletal changes and subsequent G_2/M arrest are commonly seen in apoptotic cells. However, when we performed the apoptotic assay by examining the DNA ladder, no significant apoptotic evidence was seen in mutated Cu,Zn-SOD-transfected N2a cells after 2-day serum starvation (data not shown).

The cytoskeletal changes observed in the mutated Cu,Zn-SOD in this study could be related to neuronal cell death observed in patients with FALS. In recent studies, researchers have reported that cytoskeletal proteins are significantly altered in ALS spinal motor neurons. For example, neurofilament

aggregation is known to be an early pathological hallmark of the disease process. Furthermore, Vukosavic et al. (35) reported that the level of β-actin decreases in the mutated Cu,Zn-SOD transgenic mice. The association of mutated Cu,Zn-SOD with actin reported in the present study could be an another important factor in cytoskeletal disruption and the apoptosis of neuronal cells in FALS.

The association of mutant Cu,Zn-SOD with actin could also be involved in the formation of aggregates that are observed in ALS. An increasing number of studies have stressed the role of mutant Cu,Zn-SOD-derived aggregation in the pathogenesis of ALS. Intracellular Cu,Zn-SOD aggregates are found in cultured motor neurons after the microinjection of mutant *Sod1* cDNA (11). Aggregates containing Cu,Zn-SOD were also detected in motor neurons and astrocytes of transgenic mice that expressed mutant *Sod1* (7). Mutant Cu,Zn-SOD aggregation into insoluble protein complexes is considered to be an early event in the pathogenic mechanism of FALS (18). Transfection studies indicated that mutant but not wild-type Cu,Zn-SOD forms cytoplasmic aggregates (18, 20). Such aggregates might interact inappropriately with other cellular components to impair cellular function. Pasinelli et al. (28) recently reported that mutant Cu,Zn-SOD-containing aggregates binds to Bcl-2 in spinal cord mitochondria, suggesting possible mechanisms of neurotoxicity of mutant Cu,Zn-SOD. Aggregates observed in ALS are also likely substrates for dynein-mediated transport and cause the disruption of microtubule-dependent axonal transport of other substrates. In addition, they are considered to stimulate neurodegeneration by overwhelming the capacity of the protein-folding chaperones and normal proteasome function. Thus the toxicity of mutant Cu,Zn-SOD could result from their propensity to aggregate. Similar mechanisms have been proposed for other degenerative diseases such as Alzheimer's disease, light-chain amyloidosis, and the spongiform encephalopathies (8). What, then, is the cause of the formation of such toxic aggregations? One possible mechanism is aberrant protein-protein interactions as demonstrated in mutant proteins in some neurodegenerative and/or neuromuscular disorders (9, 23). Kunst et al. (21) reported that G85R and G93A Cu,Zn-SOD bind to translocon-associated protein-δ (TRAP-δ) and lysyl-tRNA synthetase (KARS) using a yeast two-hybrid system. Although we were not able to identify TRAP-δ and KARS as proteins that bind to mutated Cu,Zn-SOD, it is possible that they were also present in the 2-D gels shown in Fig. 6. The mechanisms by which the mutated Cu,Zn-SOD associated with actin are currently under investigation. We assume that the structural changes or instability of Cu,Zn-SOD caused by the mutation suggested by the crystal structures (16) might be involved in this phenomenon. Further analysis of mutated Cu,Zn-SOD proteins will provide clues to their aberrant interactions with other proteins, including actin.

ACKNOWLEDGMENTS

We thank Dr. Yoshitaka Ikeda for technical support and critical discussion.

GRANTS

This work was supported by a grant from the Amyotrophic Lateral Sclerosis Association, a grant on Specific Diseases (Itoyama) from Ministry of Health and Welfare, Japan, the 21st Century COE Program of the Ministry of Education, Science, Culture, Sports, and Technology, and a Grant-in-Aid for Scientific Research (C) No. 15500237.

REFERENCES

1. **Andersen PM, Morita M, and Brown RH Jr.** *Genetics of Amyotrophic Lateral Sclerosis: An Overview*. London: World Federation of Neurology, Committee on Motor Neuron Disease, 1999.
2. **Arai K, Maguchi S, Fujii S, Ishibashi H, Oikawa K, and Taniguchi N.** Glycation and inactivation of human Cu-Zn-superoxide dismutase: identification of the in vitro glycated sites. *J Biol Chem* 262: 16969–16972, 1987.
3. **Banan A, Fitzpatrick L, Zhang Y, and Keshavarzian A.** OPC-compounds prevent oxidant-induced carbonylation and depolymerization of the F-actin cytoskeleton and intestinal barrier hyperpermeability. *Free Radic Biol Med* 30: 287–298, 2001.
4. **Banan A, Zhang Y, Losurdo J, and Keshavarzian A.** Carbonylation and disassembly of the F-actin cytoskeleton in oxidant induced barrier dysfunction and its prevention by epidermal growth factor and transforming growth factor alpha in a human colonic cell line. *Gut* 46: 830–837, 2000.
5. **Beckman JS, Carson M, Smith CD, and Koppenol WH.** ALS, SOD and peroxynitrite. *Nature* 364: 584, 1993.
6. **Bruijn LI, Becher MW, Lee MK, Anderson KL, Jenkins NA, Copeland NG, Sisodia SS, Rothstein JD, Borchelt DR, Price DL, and Cleveland DW.** ALS-linked SOD1 mutant G85R mediates damage to astrocytes and promotes rapidly progressive disease with SOD1-containing inclusions. *Neuron* 18: 327–338, 1997.
7. **Bruijn LI, Houseweart MK, Kato S, Anderson KL, Anderson SD, Ohama E, Reaume AG, Scott RW, and Cleveland DW.** Aggregation and motor neuron toxicity of an ALS-linked SOD1 mutant independent from wild-type SOD1. *Science* 281: 1851–1854, 1998.
8. **Bucciantini M, Giannoni E, Chiti F, Baroni F, Formigli L, Zurdo J, Taddei N, Ramponi G, Dobson CM, and Stefani M.** Inherent toxicity of aggregates implies a common mechanism for protein misfolding diseases. *Nature* 416: 507–511, 2002.
9. **Burke JR, Enghild JJ, Martin ME, Jou YS, Myers RM, Roses AD, Vance JM, and Strittmatter WJ.** Huntingtin and DRPLA proteins selectively interact with the enzyme GAPDH. *Nat Med* 2: 347–350, 1996.
10. **Cleveland DW and Rothstein JD.** From Charcot to Lou Gehrig: deciphering selective motor neuron death in ALS. *Nat Rev Neurosci* 2: 806–819, 2001.
11. **Durham HD, Roy J, Dong L, and Figlewicz DA.** Aggregation of mutant Cu/Zn superoxide dismutase proteins in a culture model of ALS. *J Neuropathol Exp Neurol* 56: 523–530, 1997.
12. **Farah CA, Nguyen MD, Julien JP, and Leclerc N.** Altered levels and distribution of microtubule-associated proteins before disease onset in a mouse model of amyotrophic lateral sclerosis. *J Neurochem* 84: 77–86, 2003.
13. **Ferrante RJ, Browne SE, Shinobu LA, Bowling AC, Baik MJ, MacGarvey U, Kowall NW, Brown RH Jr, and Beal MF.** Evidence of increased oxidative damage in both sporadic and familial amyotrophic lateral sclerosis. *J Neurochem* 69: 2064–2074, 1997.
14. **Fujii J, Myint T, Seo HG, Kayanoki Y, Ikeda Y, and Taniguchi N.** Characterization of wild-type and amyotrophic lateral sclerosis-related mutant Cu,Zn-superoxide dismutases overproduced in baculovirus-infected insect cells. *J Neurochem* 64: 1456–1461, 1995.
15. **Gurney ME, Pu H, Chiu AY, Dal Canto MC, Polchow CY, Alexander DD, Caliendo J, Hentati A, Kwon YW, Deng HX, Chen W, Zhai P, Sufit RL, and Siddique T.** Motor neuron degeneration in mice that express a human Cu,Zn superoxide dismutase mutation. *Science* 264: 1772–1775, 1994.
16. **Hart PJ, Liu H, Pellegrini M, Nersissian AM, Gralla EB, Valentine JS, and Eisenberg D.** Subunit asymmetry in the three-dimensional structure of a human CuZnSOD mutant found in familial amyotrophic lateral sclerosis. *Protein Sci* 7: 545–555, 1998.
17. **Hirano A, Nakano I, Kurland LT, Mulder DW, Holley PW, and Saccomanno G.** Fine structural study of neurofibrillary changes in a family with amyotrophic lateral sclerosis. *J Neuropathol Exp Neurol* 43: 471–480, 1984.
18. **Johnston JA, Dalton MJ, Gurney ME, and Kopito RR.** Formation of high molecular weight complexes of mutant Cu, Zn-superoxide dismutase in a mouse model for familial amyotrophic lateral sclerosis. *Proc Natl Acad Sci USA* 97: 12571–12576, 2000.
19. **Julien JP.** Amyotrophic lateral sclerosis: unfolding the toxicity of the misfolded. *Cell* 104: 581–591, 2001.
20. **Koide T, Igarashi S, Kikugawa K, Nakano R, Inuzuka T, Yamada M, Takahashi H, and Tsuji S.** Formation of granular cytoplasmic aggregates